Computers and Electronics in Agriculture 233 (2025) 110147

Contents lists available at ScienceDirect

Computers and Electronics in Agriculture

journal homepage: www.elsevier.com/locate/compag

Estimating leaf and canopy nitrogen contents in major field crops across the growing season from hyperspectral images using nonparametric regression

Dong Wang [a,b], Paul C. Struik [a], Lei Liang [b,*], Xinyou Yin [a,*]

[a] Centre for Crop Systems Analysis, Department of Plant Sciences, Wageningen University & Research, P.O. Box 430, 6700 AK Wageningen, the Netherlands
[b] Shanghai Lankuaikei Technology Development Co. Ltd., No. 888 Huanhu West 2nd Road, Pudong New District, Shanghai, China

ARTICLE INFO

Keywords:
Major crop
Nonparametric regression algorithm
Hyperspectral image
Leaf nitrogen trait
Crop nitrogen management

ABSTRACT

Estimating leaf nitrogen (N) status is crucial for site- and time-specific crop N management, and can be accomplished more routinely than ever before with the advent of hyperspectral imaging techniques. Yet, there is still a lack of information about how leaf and canopy N of major crops could be predicted from different regression methods, hyperspectral feature types, and prediction pathways. We conducted field experiments with different N supply for rice, wheat and maize, in China. Features of canopy reflectance (Ref), vegetation indices (VIs), and texture information (Tex) were extracted from acquired hyperspectral images. These features and crop developmental stage (DS) were applied to estimate crop N parameters, using five nonparametric regression algorithms: Partial Least Squares Regression (PLSR), Support Vector Regression (SVR), Random Forest Regression, Deep Neural Network, and Convolutional Neural Network. The performance of PLSR and SVR models was significantly better than that of the others when field samples were limited. Use of feature combination in leaf N prediction was identified necessary from the improved model performance after incorporating the features of Ref, Tex, and DS. The prediction of the mass-based leaf N trait, leaf N concentration, was better than that of the area-based trait, specific leaf N (SLN). Values of SLN and canopy leaf-N content were predicted comparably via themselves direct and indirect methods, although indirect procedures involved more steps requiring the prediction of two or more component traits. These results were discussed in view of making use of available regression-models, features and pathways for best predictabilities so as to improve crop N monitoring for sustainable field N management.

1. Introduction

The security and sustainability of modern agricultural production are at risk. Compared to 2000, crop production increased 50 % by 2018, while the overall fertilizer use was 40 % higher and 52 % of the increase was nitrogen (N) (FAO, 2020). Fertilization with N is needed as it strongly enhances crop growth, production and quality (Beeckman et al., 2018; Lemaire et al., 2008). However, in view of the cost of N fertilizers and the diminishing return of productivity (yield gain per unit N-fertilizer diminishes with increasing application of N), the amount of fertilizers applied to crops may be excessive (Schröder et al., 2000; Skiba, 2014). Moreover, severe environmental issues have arisen because of N losses through volatilization (Davidson, 2009), leaching (Padilla et al., 2018) and runoff (Zeng et al., 2021). Thus, it is necessary to guide farmers in performing a sustainable site- and time-specific N-fertilizer management (Weiss et al., 2020), aiming to meet crop N demands and reduce N losses to the environment simultaneously. To this end, monitoring crop N status in time is the primary step that allows the development of effective strategies for smart crop N management.

Monitoring crop N status via destructive sampling and biophysical or chemical analyses is costly and time consuming. Remote sensing has emerged as a relatively cheap and fast method to monitor crop N status. The monitoring of the aboveground N content in leaves of a canopy (N_{leaves}) is crucial as it determines canopy photosynthetic capacity and thus crop productivity (Peng et al., 1995). Since N_{leaves} is the integration of N content of individual leaves in a canopy, it is also necessary to monitor the status of leaf N, such as specific leaf N content (SLN, g N m^{-2}) that has been widely used as a parameter to calculate leaf photosynthesis rate (Evans, 1983; Wang et al., 2022; Yin et al., 2009). Investigating SLN is supported by the expectation that the light reflected or transmitted by a leaf is considered to interact within the whole leaf thickness in spectral domains of absorption. Thus, the reflectance (Ref)

* Corresponding authors.
E-mail addresses: lei.liang@lankuaikei.cn (L. Liang), xinyou.yin@wur.nl (X. Yin).

https://doi.org/10.1016/j.compag.2025.110147
Received 14 August 2023; Received in revised form 19 January 2025; Accepted 16 February 2025
Available online 24 February 2025

and transmittance are supposed to be more directly sensitive to the variation in the area-based content of absorbing constituents, like SLN, but rather less to the mass-based leaf N concentration (LNC, g g^{-1}) (Baret and Fourty, 1997). However, it is surprising that the estimation of SLN is still rare (Berger et al., 2020b), whereas there are many studies regarding the prediction of LNC from remote sensing images (e.g., Moharana and Dutta, 2016; Raj et al., 2021). Among the few studies comparing the prediction of SLN and LNC, the results were inconsistent (Ecarnot et al., 2013; Li et al., 2018).

The N status at canopy or leaf scale could be derived from hyperspectral images either directly or using an indirect prediction pathway. The latter is possible because, for example, SLN can be calculated from LNC and the leaf thickness parameter "specific leaf weight" (SLW, g m^{-2}) (Baret and Fourty, 1997) or its reciprocal "specific leaf area" (SLA, m^2 g^{-1}). The SLN in wheat was shown being better predicted by the indirect approach than by the direct method (Ecarnot et al., 2013). Given that such studies are few and show inconsistent results in predicting SLN and LNC, indirect and direct approaches in predicting nitrogen contents at both leaf and canopy scales (SLN and N_{leaves}, respectively) should be further evaluated.

Regression methods relating to N prediction from remote sensing have been developed since the pioneering work by Thomas and Oerther (1972). Generally, predicting methods can be classified into four categories: parametric regression methods like methods based on vegetation indices (VIs), nonparametric regression methods including linear and nonlinear regression algorithms, physical methods like inversion of radiative transfer models, and hybrid regression methods by combining physically based methods with nonparametric regression methods (Verrelst et al., 2019). Nonparametric regression methods, which explore the direct link between target traits and the given spectral data, are recently receiving more attention than the other three methods (Berger et al., 2020b). Regression algorithms like Partial Least Squares Regression (PLSR), Support Vector Regression (SVR) and Random Forest Regression (RFR) have been employed in recent studies (Wang et al., 2021; Yao et al., 2015). However, deep learning-based regression methods, such as Deep Neural Network (DNN) and Convolutional Neural Network (CNN), are still under-utilized for crop N prediction based on canopy-level hyperspectral Ref (Fu et al., 2020). Given that DNN has shown more potential than other regression methods in combining different types of features (Maimaitijiang et al., 2020), predicting leaf and canopy N by deep learning-based regression algorithms are also worthy to be explored.

Regarding the features, spectrum and texture are fundamental pattern elements in imagery interpretation. The full spectrum has been widely used in chemometrics (Atzberger et al., 2010). The shortwave infrared region (SWIR, 1300 to 2500 nm) has been explored for leaf N monitoring (Berger et al., 2020b; Kokaly et al., 2009). However, its lower solar energy flux and signal-to-noise ratio (Guanter et al., 2015) may cause significant uncertainties in prediction (Féret et al., 2021). In comparison, the spectrum within visible (400 to 700 nm) and near infrared (NIR, 750 to 1300 nm) regions, and the so-called red-edge (680 to 750 nm where there is a sharp change in leaf Ref), have a strong optical signal for crop N estimation by chlorophyll pigments (e.g., Horler et al., 1983; Homolová et al., 2013). For instance, although only representing 1.7 % of the total leaf N (Kokaly et al., 2009), leaf pigments contribute predominantly to the canopy Ref within the visible region (Fu et al., 2020). While spectral features describe the variations in various bands of an electromagnetic spectrum, textural features contain the information about the spatial characteristics of canopy architecture within a band (Colombo, 2003; Haralick et al., 1973). Fusing canopy texture information (Tex) together with spectral features is therefore gaining momentum in phenotyping crop traits such as leaf area index (LAI) (Liu et al., 2021), biomass (Zheng et al., 2018b; Liu et al., 2022), and yield (Maimaitijiang et al., 2020). Meanwhile, Zheng et al. (2018a) also showed that LNC in rice was better predicted after incorporating Tex into VIs. As crop N status varies along with leaf area expansion, biomass accumulation and grain formation (e.g., Ohyama, 2010), combining Ref and Tex together is expected to capture the changes of canopy and leaf N as well.

Although spectral and textural features vary with crop status within the growing season, it has been claimed that stage-specific regression models should be developed and tested for better prediction of crop status (e.g., Barbedo, 2019). However, such models may lack the ability to be applied temporally at any growth stage. To overcome this, Li et al. (2022) successfully incorporated developmental stage (DS) into VI-based models to estimate wheat biomass over the entire growing season. Yet, the potential of utilizing DS in whole-season crop N monitoring is still unknown. Furthermore, taking advantage of high spatial (< 1 m) and spectral (< 10 nm) resolution of the Unmanned Aerial Vehicle (UAV)-acquired hyperspectral images, combining DS with canopy hyperspectral features is supposed to better predict leaf and canopy N in site-specific field N management. This particularly meets the needs of smallholders, especially in China, where the area of a typical farm is only $\sim$ 0.1 ha and its width is often less than 7 m (Chen et al., 2011; Zhang et al., 2013).

The above overview highlights the plethora of available tools in terms of regression models, features and pathways to predict canopy and leaf N. It is important to explore a best scenario for prediction, conditional on a limited size of data commonly collected from field experiments for crops. In this study, canopy and leaf N traits from hyperspectral images are predicted by combining canopy Ref, VIs, Tex and crop DS by five nonparametric regression algorithms for three major crops (rice, wheat, maize). Our objectives are: 1) to explore the combined utilization of different feature types and regression algorithms in the prediction of crop N traits at leaf level, SLN and LNC, and at canopy level, N_{leaves}, in different crop species; 2) to compare and identify the effective pathways (direct vs. indirect) in obtaining N traits of major crops. Achieving these objectives would help monitor crop N status for more accurately predicting crop growth and guide N-fertilizer management in the context of sustainable precision agriculture.

2. Materials & methods

2.1. Experimental design

Field experiments with different N rates from deficient to excessive were conducted in China: the rice experiment was in Chongming, Shanghai, while the maize and winter wheat experiments were in Luohe and Zhoukou, respectively, Henan province (Fig. 1). Treatments for each experiment were arranged as a randomized block design. There were four replications (four blocks) in the rice experiment, and within each block, six N rates, varying from 0 to 320 kg N ha^{-1}, were applied to rice (cultivar: Nanjing 46), planted on 4 June 2020 with a row spacing of 20 cm and a within-row plant spacing of 2.5 cm. The plot size was 6×30 m^2. The experiments on maize (cultivar: Zhengdan 958) and winter wheat (cultivar: Bainong 4199) were designed with eight blocks, and in each block seven N rates, varying from 0 to 400 kg N ha^{-1}, were applied. Each plot of maize was 10×20 m^2 and each plot of wheat was 9×18 m^2 (Fig. 1). Maize was sown on 9 June 2020 with 60 cm row spacing and 25 cm plant spacing within the row. Winter wheat was planted on 24 October 2020 with a row spacing of 21 cm and a within-row plant spacing of 1.5 cm. Urea N fertilizer (N, 46 %) was split-applied according to the rate and the time schedule described in Table S1. Based on the local practice, for each experiment, sufficient phosphate (112.5, 120 and 75 kg P_2O_5 ha^{-1} for rice, maize and winter wheat, respectively) and potash (112.5, 120 and 105 kg K_2O ha^{-1} for rice, maize and winter wheat) fertilizers were applied. Irrigation, and pest, disease and weed control were the same for all treatments within a crop species and followed local standard practices.

The overall procedure used in this study is given in Fig. 2, in which we particularly showed direct and indirect pathways predicting SLN and N_{leaves}. The SLN directly predicted from hyperspectral images (SLN_{dir})

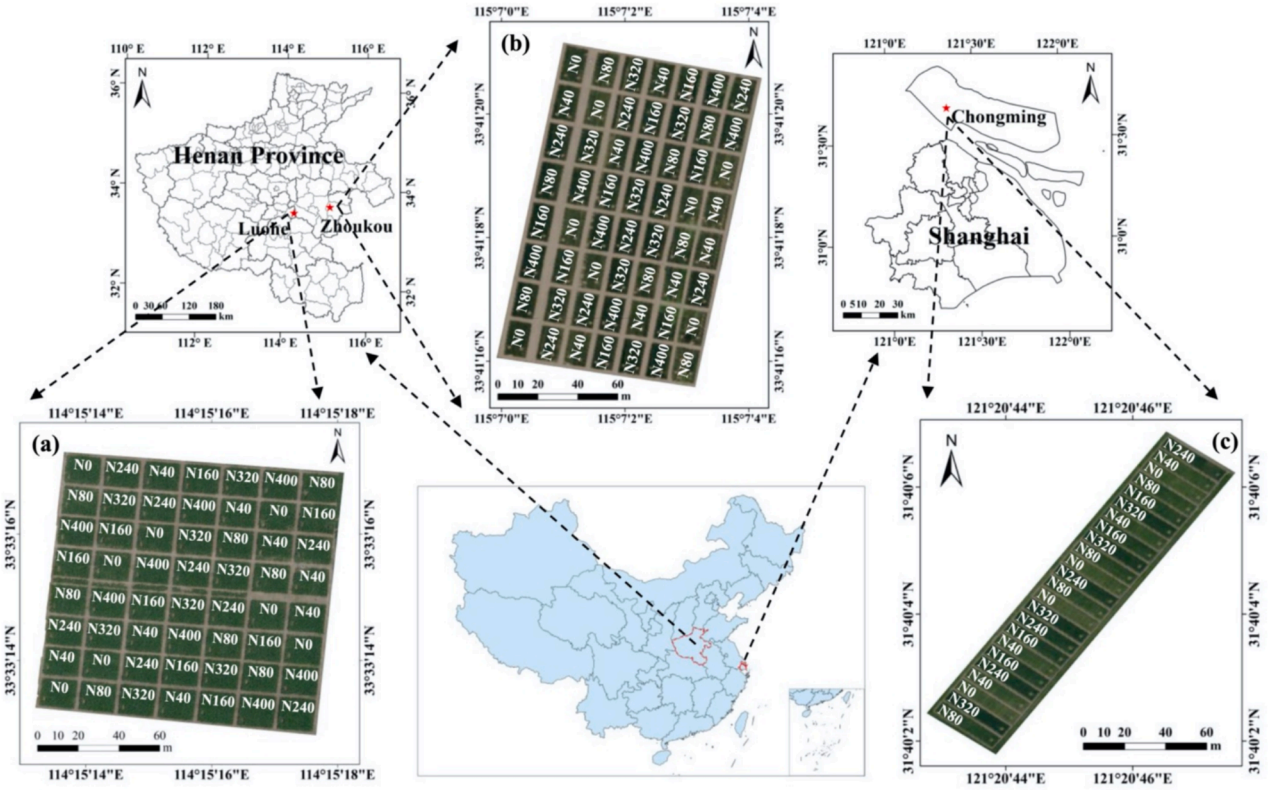

Fig. 1. Study sites of the field experiments of maize (a), wheat (b) and rice (c). The true color images (Red: 638 nm, Green: 550 nm, Blue: 470 nm) at the stem-elongating stage are illustrated here. N0, N40, N80, N160, N240, N320 and N400 denote different nitrogen (N) application rates (see Table S1 for details).

was distinguished from the indirectly predicted SLN (the predicted LNC divided by the predicted SLA, SLN_{sla}; the predicted LNC multiplied by the predicted SLW, SLN_{slw}). Thereafter, three indirect pathways for predicting N_{leaves} (the product of SLN_{dir}, SLN_{sla} or SLN_{slw} with the predicted LAI, $N_{leaves,SLNdir}$, $N_{leaves,SLNsla}$ or $N_{leaves,SLNslw}$, respectively), were compared with the directly predicted N_{leaves} ($N_{leaves,dir}$). The acronyms of the targeted leaf traits at the leaf and canopy levels are summarized in Table 1.

2.2. Data acquisition

2.2.1. Canopy leaf trait measurements

Crops were destructively sampled from all experimental plots on six dates (Table 2). At each sampling date, aboveground plants were cut within an area of 2.25, 1.0, and 2.4 m^2 in each plot for rice, wheat and maize, respectively. The total fresh samples were weighed immediately and about 20 % of the biomass was used as sub-sample to be dissected into component plant parts, including green leaves, stems, and grains. Yellow leaves were not included. Leaf area of the dissected sub-sample was measured on one-side of the fresh green leaves using a LI-3100C Area Meter (Li-Cor, Lincoln, NE, USA). The leaf area of the measured sub-sample was converted to that of the total-sample acquired in each plot, according to the ratio of sub-sample to total-sample biomass, and then divided by the total sampling area to get the LAI. Then, green leaves were weighed after being oven-dried at 70 °C to constant weight. All green leaves belonging to same sample were mixed and ground, and then stored for chemical analysis. LNC, expressed on the basis of leaf dry weight, was determined by the Micro-Kjeldahl method. N_{leaves} was calculated as the product of LNC and leaf weight per unit ground area. SLW was calculated as the ratio of leaf weight to leaf area measured by LI-3100C, and SLA was calculated as 1/SLW. SLN was calculated as the product of LNC and SLW. Data records of wheat at maturity were excluded in this study, as there were no green leaves remaining at that time.

2.2.2. Canopy reflectance measurements

Canopy Ref data were obtained before each field destructive sampling by a Cubert S185 hyperspectral snapshot camera (Cubert GmbH, Ulm, Baden-Württemberg, Germany). The camera was equipped with a DJI Ronin-MX three-axis gimbal stabilizer and installed on a DJI M600 PRO hexacopter with a global positioning system (GPS) and inertial navigation system modules (DJI, Shenzhen, China). The gimbal stabilizer ensured that the view angle of the camera was constant, which contributed to the acquisition of the nadir images. The camera captures 125 spectral bands in the range of 450–950 nm with a sampling interval of 4 nm. The light is split into two beams after passing through the camera lens. 80 % of the entire light entering the camera creates a 50 × 50 pixels hyperspectral cube with a 12-bit dynamic range and the remaining 20 % enters the panchromatic camera to create a panchromatic image with a resolution of 1000 × 1000 pixels (e.g., Aasen et al., 2015; Lu et al., 2020). After pan-sharpening the hyperspectral cube to the resolution of panchromatic image by the Cube-Pilot software (Cubert GmbH, Ulm, Baden-Württemberg, Germany), hyperspectral images with a size of 1000 × 1000 pixels can be generated.

The flight campaigns were performed between 10 a.m. and 2 p.m. in consistent weather conditions (cloudless or heavy cloud) to minimize changes in illumination. The hyperspectral camera was calibrated by a white and black board before flying. The flight height was 60 m, resulting in a spatial resolution of about 2 cm, and the flying speed was fixed at 6 m s^{-1}. The hyperspectral images were created automatically at a sampling time interval of 1 ms and the forward and side overlaps were set to 80 % and 60 %, respectively, under the control of a connected microcomputer. The images were orthographically stitched by the Agisoft PhotoScan software (Agisoft LLC, St. Petersburg, Russia) based on GPS coordinates or image textures. Finally, the region of interest was drawn from the sampling area on the obtained hyperspectral *ortho-*

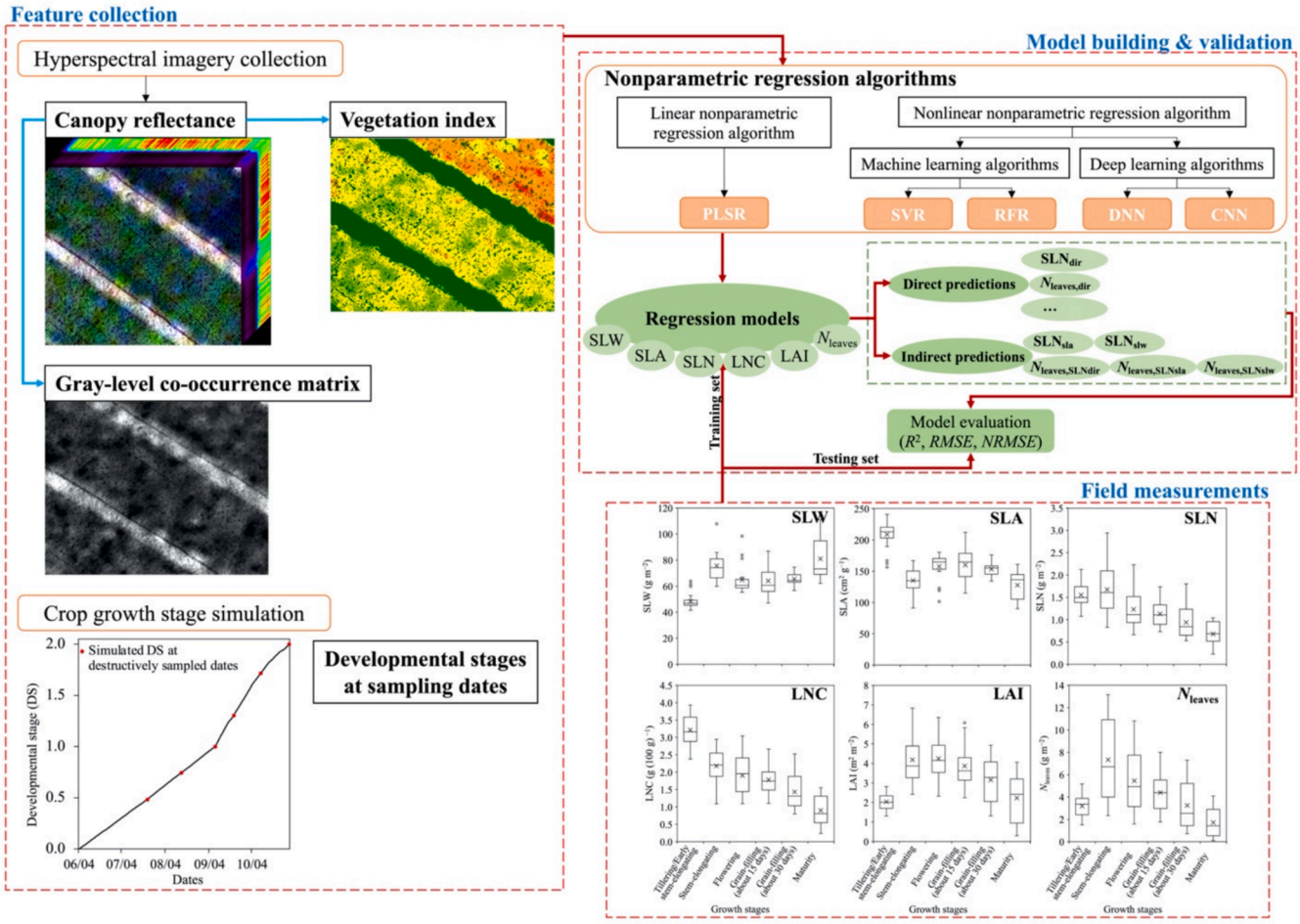

Fig. 2. The workflow diagram of data acquisition, feature collection, and data analysis in this study. Nonparametric regression algorithms are: PLSR = Partial Least Squares Regression, SVR = Support Vector Regression, RFR = Random Forest Regression, DNN = Deep Neural Network, CNN = Convolutional Neural Network. Crop traits are: SLW = specific leaf weight, SLA = specific leaf area, SLN = specific leaf nitrogen, LNC = leaf nitrogen concentration, LAI = leaf area index, N_{leaves} = nitrogen content in leaves of the canopy. $N_{leaves,dir}$ and SLN_{dir} represent the direct predictions of N_{leaves} and SLN, respectively. Within the indirect predictions, SLN_{sla} was calculated as the predicted LNC divided by the predicted SLA, and SLN_{slw} was calculated as the product of the predicted LNC and SLW; $N_{leaves,SLNdir}$, $N_{leaves,SLNsla}$, and $N_{leaves,SLNslw}$ were derived from predicted LAI and SLN_{dir}, LAI and SLN_{sla}, and LAI and SLN_{slw}, respectively (see also Table 1).

images. The mean spectrum of the destructive sampling area was used as the corresponding Ref of each sample. The bands beyond 902 nm and below 470 nm were dropped in the later data analysis, due to the low spectral quality (Lu et al., 2020).

2.3. Features collections for leaf traits prediction

2.3.1. Canopy spectral features and vegetation indices

The raw bands from hyperspectral images were used as canopy spectral features. Additionally, in our study, 37 narrowband hyperspectral VIs were collected, in which 6 were directly related to N, 16 were related to chlorophyll, and 15 were related to canopy traits like biomass, coverage or LAI (Table S2). One more red-edge position was added in the list of VIs (Table S2), which was regressed by the inverted Gaussian method (Miller et al., 1990). The wavelengths with the sampling interval of 4 nm in our study were linearly interpolated to 1 nm to match the needs of calculation of hyperspectral VIs.

2.3.2. Canopy texture information extraction

Texture information (Tex) from each hyperspectral band was extracted by the commonly used grey level co-occurrence matrix algorithm (Haralick et al., 1973). Eight texture features, including mean, variance, homogeneity, contrast, dissimilarity, entropy, second moment and correlation, were computed using the ENVI 5.2 software (Exelis Visual Information Solutions, Boulder, Colorado, USA). To avoid complexity of computation, only four bands, 470, 550, 638, and 850 nm (representative wavelengths for blue, green, red, and NIR regions, respectively; e.g., Blackburn, 1998; Zheng et al., 2018b) were selected here for canopy Tex extraction.

2.3.3. Crop developmental stage

As leaf traits were measured at various dates during crop growth and these traits varied in time, we included crop DS as a co-predictor. It was simulated by the crop growth simulation model GECROS (Yin and van Laar, 2005; Yin and Struik, 2017), in which the DS at seedling emergence, flowering and maturity were denoted as dimensionless values 0.0, 1.0 and 2.0, respectively, and the effect of temperature fluctuations on rate of crop development was taken into account. A brief description of the GECROS model for simulation of DS is provided in the Supplement Text A. The related parameters used in DS simulation are listed in Table S3.

2.4. Nonparametric regression algorithms

The commonly used linear nonparametric regression algorithm PLSR, two machine learning algorithms SVR and RFR, and two deep learning-based algorithms DNN and CNN were implemented in the canopy leaf traits predictions (Fig. 2).

Table 1
List of acronyms of leaf traits at the leaf and canopy level with their definitions or calculations, and units.

Acronym	Definition or calculation	Unit
LAI	Leaf area index	m^2 leaf (m^2 ground)$^{-1}$
LNC	Leaf nitrogen concentration	g N (g dry matter)$^{-1}$
SLA	Specific leaf area	m^2 leaf (g dry matter)$^{-1}$
SLN	Specific leaf nitrogen content	g N (m^2 leaf)$^{-1}$
SLN_{dir}	SLN directly predicted from hyperspectral images	g N (m^2 leaf)$^{-1}$
SLN_{sla}	SLN indirectly predicted as the predicted LNC divided by the predicted SLA	g N (m^2 leaf)$^{-1}$
SLN_{slw}	SLN indirectly predicted as the product of the predicted LNC and SLW	g N (m^2 leaf)$^{-1}$
SLW	Specific leaf weight (= 1/SLA)	g dry matter (m^2 leaf)$^{-1}$
N_{leaves}	Nitrogen content of leaves in the canopy	g N (m^2 ground)$^{-1}$
$N_{leaves,dir}$	N_{leaves} directly predicted from hyperspectral images	g N (m^2 ground)$^{-1}$
$N_{leaves,SLNdir}$	N_{leaves} indirectly predicted as the product of SLN_{dir} and the predicted LAI	g N (m^2 ground)$^{-1}$
$N_{leaves,SLNsla}$	N_{leaves} indirectly predicted as the product of SLN_{sla} and the predicted LAI	g N (m^2 ground)$^{-1}$
$N_{leaves,SLNslw}$	N_{leaves} indirectly predicted as the product of SLN_{slw} and the predicted LAI	g N (m^2 ground)$^{-1}$

2.4.1. Partial Least Squares Regression (PLSR)

PLSR is characterized by the ability to perform regression modeling even when the independent variables have severe multiple correlations, or even when there are fewer sample points than given variables. Therefore, it allows all original independent variables being included in the final model (Geladi and Kowalski, 1986). The only hyperparameter in PLSR optimized in this study was the number of potential components ("n_components", Table S4).

2.4.2. Support Vector Regression (SVR)

SVR has unique advantages in the case of small samples as well as nonlinear and high-dimensional inputs (Drucker et al., 1997). It improves the predictability by mapping low-dimensional samples into high-dimensional space and thus the non-linear inputs can be linearly separated by using a kernel function. SVR is efficient in finding sample information to achieve the best compromise between model complexity and learning ability.

2.4.3. Random Forest Regression (RFR)

RFR is a robust ensemble learning technique able to manage large numbers of input variables. RFR combines a large set of decision trees (Breiman, 2001). Together with the number of trees, tree traits and the number of input features can be optimized to get the best model (Table S4).

2.4.4. Artificial Neural Networks (ANNs)

Normally, an ANN is composed of an input layer, several hidden layers and an output layer and each layer contains a number of neurons. In this study, the fully connected feedforward DNN is based on simply increasing the depth (number of layers) of ANNs (Längkvist et al., 2014) (Fig. S1a). Fully connected 1-D CNN with several layers of convolution and pooling was designed as well (Fig. S1b). The stacked multiple layers are able to extract higher-order feature information (Längkvist et al., 2014). The optimum composition of hidden layers was determined by the minimum value of the root mean square error (*RMSE*) in validation dataset, while the number of neurons in each layer was asserted beforehand. Herein, the selected activation function for hidden layers was the Rectified Linear Unit with the form of $f(z) = \max(0, z)$ (LeCun et al., 2015). The weights of model neurons were initialized by the initialization method of He et al. (2015) and then updated by applying the gradient descent algorithm of the Adam optimizer. A reduced learning rate on plateau and early stopping were implemented as well to prevent overfitting.

2.5. Model implementation and performance evaluation

The prepared feature information, including canopy Ref, hyperspectral VIs, Tex, and DS, was selectively assembled and then compressed into a one-dimensional vector as the feature set (Table 3). Three procedures were used to implement each of the above regression algorithms. First, for each crop, random assignment of instances was used for splitting the training and testing data, in which 75 % of the data per growth stage was randomly selected as the training dataset and the remaining 25 % was used as the testing set. The selected training data across stages were pooled to build the full-growth-stage models per crop, which were then validated against the pooled data of the testing set across stages of the crop. Secondly, for each crop, regression algorithms were developed, in which feature sets were selected using all data except for one stage. Then the model performance was evaluated by the growth stage which was not used in the model training. Thirdly, regression algorithms were trained by combining data of the crops, except for one crop whose data were then used to test the model performance. The second and the third procedures, also referred to as leave one stage out procedure and leave one crop out procedure, respectively, allowed to further evaluate model predictabilities across stages and across crops correspondingly.

All data analysis and model training were conducted in the Python environment. Regression models were implemented relying on the package of scikit-learn (0.24.1) (Pedregosa et al., 2011) and TensorFlow

Table 3
Description of the combinations of feature sets from hyperspectral images and crop model simulations.

Acronym	Feature type	Feature number
Ref	Canopy reflectance	109
RefVIs	Canopy reflectance + Vegetation indices	147
RefTex	Canopy reflectance + Texture information	141
RefTexDS	Canopy reflectance + Texture information + Developmental stage	142

Table 2
Sampling dates and the number of destructive field samples at corresponding growth stages of rice, maize and wheat.

Growth stage	Rice		Maize		Winter wheat	
	Sampling date	Number of samples	Sampling date	Number of samples	Sampling date	Number of samples
Tillering stage/Early stem-elongating stage	22 July	24	7 July	19	22 March	56
Stem-elongating stage	15 August	24	20 July	19	8 April	56
Flowering stage	8 September	24	4 August	19	27 April	56
Grain-filling stage	21 September	24	25 August	19	10 May	56
Grain-filling stage	10 October	24	7 September	19	25 May	56
Maturity	30 October	24	23 September	18	4 June	–
Total number of samples		144		113		280

(2.5) (Abadi et al., 2015) in Python. Table S4 gives the specific properties and numerical settings of the hyperparameters for each regression algorithms. *K*-fold cross validated *RMSE* was minimized to tune the pivotal hyperparameters in machine learning models. The method of Z-standardization was adopted to standardize model inputs during model training and testing.

The performances of all models were evaluated by the results in the testing sets (unless specified otherwise), with the coefficient of determination (R^2) and the normalized root mean square error (*NRMSE*), with the following equations:

$$R^2 = 1 - \frac{\sum_{i=1}^{n}(y_i - \hat{y}_i)^2}{\sum_{i=1}^{n}(y_i - \bar{y})^2}$$

$$NRMSE(\%) = \frac{\sqrt{\frac{1}{n}\sum_{i=1}^{n}(y_i - \hat{y}_i)^2}}{y_{max} - y_{min}} \times 100$$

where $\hat{y}_i$ is a predicted value, y_i is a measured value, y_{max} and y_{min} are the maximum and minimum of measured values of the dependent variable across the whole growing season, and n is the number of measurements. The *NRMSE* was applied here (instead of *RMSE*) as the metric of model performance evaluation because *NRMSE* has no unit, allowing comparisons of prediction errors among crops or among traits.

The Student's *t*-test was conducted to compare pairs (e.g., between modeled and measured traits) for significance of differences. When the comparison involved more than a pair (e.g., to examine predictive differences among regression methods, or among feature sets), an honest significant difference (HSD) Tukey's test was conducted following one-way analysis of variance.

3. Results

3.1. Canopy spectral reflectance and canopy and leaf N traits

Differences in canopy Ref were observed across growth stages in the three crop species and the change tended to be similar in rice and wheat (Fig. 3a–c). Values of SLN in rice and wheat became lower with the progress of the growth stage, but SLN in maize even increased at maturity (Fig. 3d), which might be caused by the rapid decline in LAI associated with senescence of the upper leaves while the cob leaves remained green (Fig. S2). Values of LNC decreased from the tillering stage of rice and wheat or the early stem-elongating stage of maize onwards (Fig. 3e). Measured N_{leaves} in both rice and wheat reached the peak at the stem-elongating stage and then decreased until maturity, while the highest values of N_{leaves} in maize occurred at flowering (Fig. 3f). Unlike in rice and wheat, there was no significant difference in measured SLN, LNC and N_{leaves} between treatments in maize (results not shown), presumably because the residual N supply from soil was very high.

3.2. Correlograms of collected features with respect to leaf and canopy N traits

Among the three crops, the correlation coefficients (r) of N_{leaves} with canopy Ref changed in a similar trend and slightly decreased when wavelength was between 680 nm and 710 nm, which belongs to the red-edge region (Fig. S3). SLN and LNC in rice showed weaker correlations than N_{leaves} with canopy Ref in the NIR region and the r ranged from 0.15 to 0.27 and from − 0.06 to 0.11, respectively (Fig. S3a). Within the

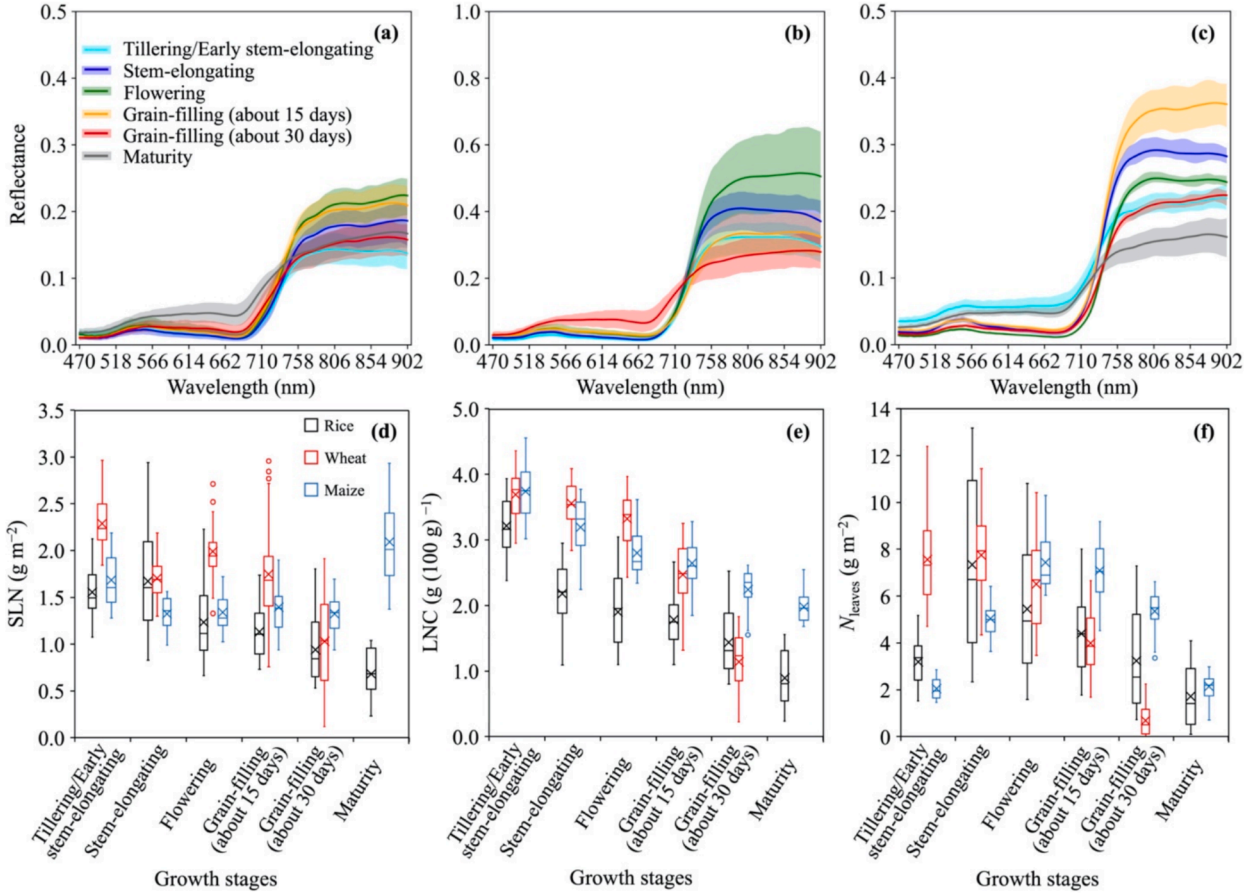

Fig. 3. Range of the collected canopy reflectance of rice (a), wheat (b) and maize (c), and the data distribution of destructively sampled specific leaf nitrogen (SLN) (d), leaf nitrogen concentration (LNC) (e), and nitrogen content in leaves of the canopy (N_{leaves}) (f) at different stages during the whole growing season.

collected VIs, the highest values of r for SLN, LNC and N_{leaves}, with VIs were up to 0.77, 0.86 and 0.82 in rice, and 0.72, 0.93 and 0.95 in wheat (Fig. S4a-f). In maize, LNC displayed a weak correlation with collected VIs and the r ranged from − 0.37 to 0.40 (Fig. S4g-i).

Regarding correlations with the Tex, leaf N traits were more correlated with the features extracted from blue, green and red bands than those from NIR in rice (Fig. S5a-d), while the higher correlations tended to be achieved from the bands of red and NIR in wheat and maize (Fig. S5e-l). The LNC in maize was highly correlated with the Tex from the NIR band and the highest value of r was up to 0.81 (Fig. S5l).

3.3. Performance of nonparametric regression algorithms and input feature sets

To comprehensively evaluate the model performance using different regression algorithms and input feature sets, three procedures were implemented. Within the first procedure, the random split of destructive samplings across each growth stage was applied to develop full-growth-stage models for leaf and canopy N traits, including SLN, LNC and N_{leaves}. As VIs were calculated from Ref (Table S2), hardly any additional information was provided via further incorporating VIs into the feature set of Ref that possessed high spectral resolution. This was supported by the results that there was no significant difference in prediction performance between Ref and RefVIs in both training and test datasets (Fig. S6). Therefore, the rest of data analysis was only focused on the feature set of Ref, RefTex and RefTexDS. After incorporating Tex and DS into the feature set of Ref, the quality of the predictions of N traits improved (Fig. 4, Fig. S7). Yet, there was no significant ($p > 0.05$) difference in the *NRMSE* of the predicted leaf N traits among different feature sets. Regarding the regression algorithms, RFR performed best in the training set for the three crop species (Fig. 5a–c), albeit worse than PLSR and SVR in the testing set (Fig. 5d–f). Although DNN and CNN occasionally performed better than other regression algorithms (Fig. 4, Fig. S7), their performance lacked the consistency in both training and testing datasets of canopy and leaf N traits of the three crops (Fig. 5).

Two additional procedures were conducted to further investigate the predictability of the regression algorithms and features sets, in which their performances at different growth stages and for three crop species were validated. In line with the first procedure, the feature sets performed comparably ($p > 0.05$) in both the leave one stage out procedure and the leave one crop out procedure for the prediction of canopy and leaf N traits. As for validating across growth stages in the leave one stage out procedure, RFR performed better than the other algorithms in the training set (Fig. 6a–c). Especially PLSR and SVR performed better than the other algorithms in testing sets and their *NRMSE* values were significantly ($p < 0.05$) lower than those of DNN and CNN (Fig. 6d–f). Regarding the leave one crop out procedure that validates across crop species, RFR performed significantly the best (Fig. 7a–c) in training,

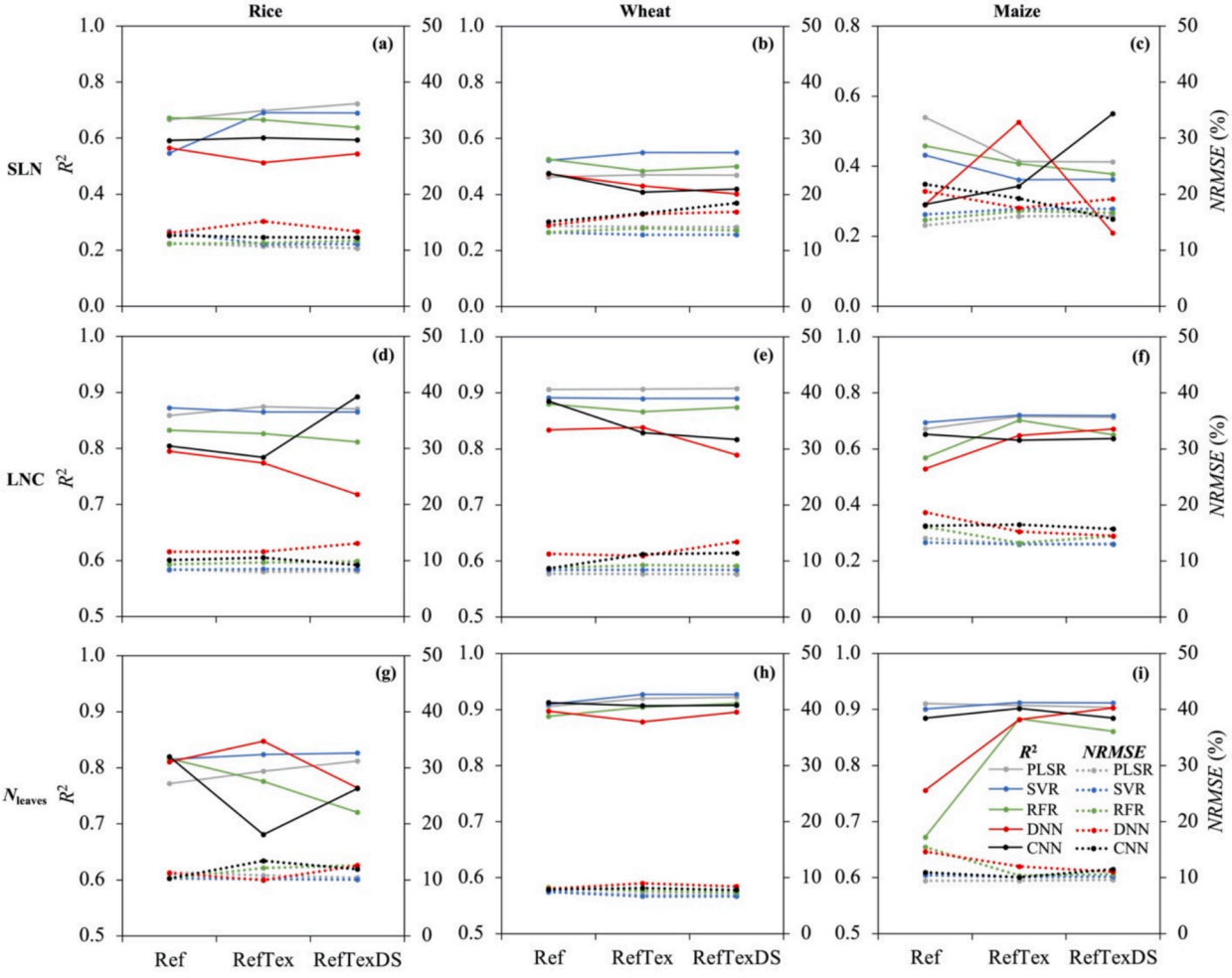

Fig. 4. The prediction performance in the testing dataset of different regression algorithms and various sets of input feature types, under the procedure of the random split of destructive samplings across each growth stage. The R^2 (full lines) and *NRMSE* (dotted lines) of directly predicted specific leaf nitrogen (SLN) (a-c), leaf nitrogen concentration (LNC) (d-f) and nitrogen content in leaves of the canopy (N_{leaves}) (g-i) are shown for rice, wheat and maize. Nonparametric regression algorithms: PLSR = Partial Least Squares Regression, SVR = Support Vector Regression, RFR = Random Forest Regression, DNN = Deep Neural Network, CNN = Convolutional Neural Network. Acronyms in the x-axis for the three sets of feature types are defined in Table 3.

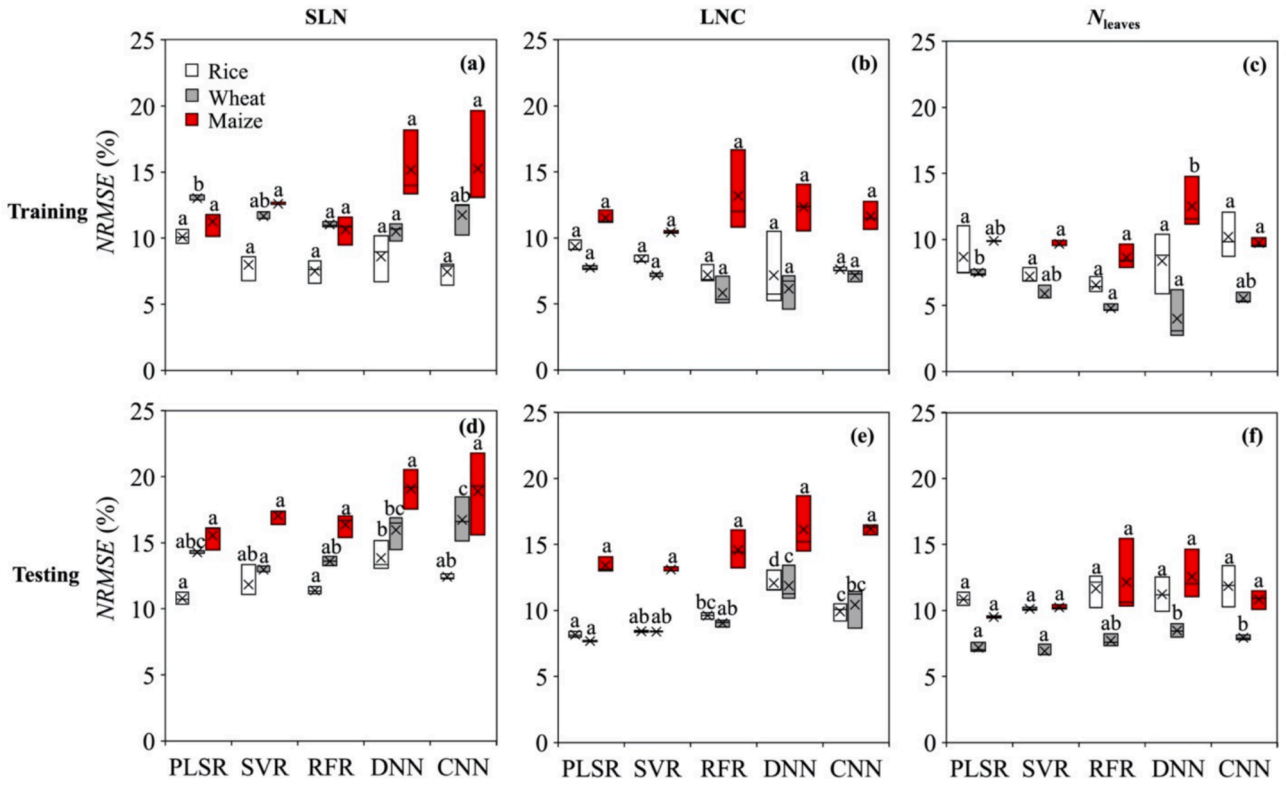

Fig. 5. The prediction performance of different regression algorithms under the procedure of the random split of destructive samplings across each growth stage for each crop. The boxplots of *NRMSE* of different regression models are shown for specific leaf nitrogen (SLN) (a, d), leaf nitrogen concentration (LNC) (b, e) and nitrogen content in leaves of the canopy (N_{leaves}) (c, f) in the training and testing datasets. In each boxplot point, the cross mark represents the mean value, while the vertical spead represents the variability, of *NRMSE* arising from using three feature sets. The different letters (a, b and c) above the bars indicate significant differences of prediction performance between regression models according to the HSD Tukey's test. Nonparametric regression algorithms: PLSR = Partial Least Squares Regression, SVR = Support Vector Regression, RFR = Random Forest Regression, DNN = Deep Neural Network, CNN = Convolutional Neural Network.

although its performance tended to be comparable to that of other algorithms in testing sets (Fig. 7d–f). Compared with the *NRMSE* of the full-growth-stage models derived from the first procedure (Fig. 5), the predicted N_{leaves} differed more from the measurements in the testing sets when validating across growth stages (Fig. 6d–f) and crop species (Fig. 7d–f). This analysis indicates low transferability of data sets from one crop to another or from one stage to another, and thus, unless specified, the results of the leave one stage out procedure and the leave one crop out procedure will no longer be used.

3.4. Performance in modeling canopy and leaf N by direct and indirect predictions

Noticeably, within the first procedure, the predicted LNC agreed with its measurements better than the predicted SLN across the three crop species (Fig. 4a–f, Fig. S7a-f, Fig. S8). To get a best predicted SLN, three prediction pathways for SLN were compared, including the directly predicted SLN_{dir}, and the indirectly predicted SLN_{sla} and SLN_{slw} (Table 1). Based on the results in the above section, the regression algorithms of PLSR and SVR were selected to conduct the comparison (Table 4). Although the predicted SLA agreed with its measurements better than was the case for SLW (Fig. S9), the indirect prediction pathways of SLN were comparable ($p > 0.05$) to each other using PLSR or SVR in the three crops. They also performed comparably to the directly predicted SLN_{dir}. Similar with the SLN_{dir}, the incorporation of feature sets also improved the prediction performance of SLN_{sla} and SLN_{slw} by PLSR and SVR in the three crops (Table 4). The *NRMSE* of the predicted SLN from different pathways using RefTexDS was significantly ($p < 0.05$) lower than that using Ref in rice. Especially in the indirect prediction pathways of SLN, RefTexDS systematically performed the best in comparison with Ref and RefTex in the three crops and for the two regression algorithms. Moreover, the *NRMSE* of SLN_{sla} and SLN_{slw} using the feature set of RefTexDS was also consistently lower than that of SLN_{dir} (Table 4).

Like the predicted SLN from different pathways, four prediction pathways for N_{leaves} were compared, namely the directly predicted $N_{leaves,dir}$ and the indirectly predicted $N_{leaves,SLNdir}$, $N_{leaves,SLNsla}$ and $N_{leaves,SLNdir}$ (Table 1). To upscale the predicted SLN to N_{leaves} in the indirect pathways, LAI was predicted as well while applying the regression algorithms of PLSR and SVR (Fig. S10). In both training and testing sets across the three crops, the predicted N_{leaves} from the four pathways differed insignificantly ($p > 0.05$), except for that of maize in the training set and that of wheat in the testing set using SVR (Fig. S11). Additionally, within the comparison of prediction pathways of N_{leaves}, the performance of PLSR and SVR was also comparable ($p > 0.05$), except for that in the training set of wheat (Fig. S11). Using more features from Ref to RefTexDS universally improved directly or indirectly predicted N_{leaves} (Fig. 8), and especially, the predictions from RefTexDS significantly ($p < 0.05$) decreased the *NRMSE* compared with those from Ref in rice and wheat using PLSR (Fig. 8). Within the comparison among feature sets, the predicted N_{leaves} using SVR agreed with the measurements significantly ($p < 0.05$) better than that using PLSR in the three crops in the training sets (Fig. 8a–c). In the testing sets, the N_{leaves} tended to be better predicted via PLSR (Fig. 8d–f), although the differences were insignificant ($p > 0.05$). For instance, compared with using SVR, *NRMSE* of N_{leaves} from different prediction pathways using PLSR on average decreased from 10.5 %, 7.6 % and 9.9 % to 10.3 %, 7.0 % and 9.3 % for rice, wheat and maize, respectively, while applying the feature set of RefTexDS (Fig. 8d–f).

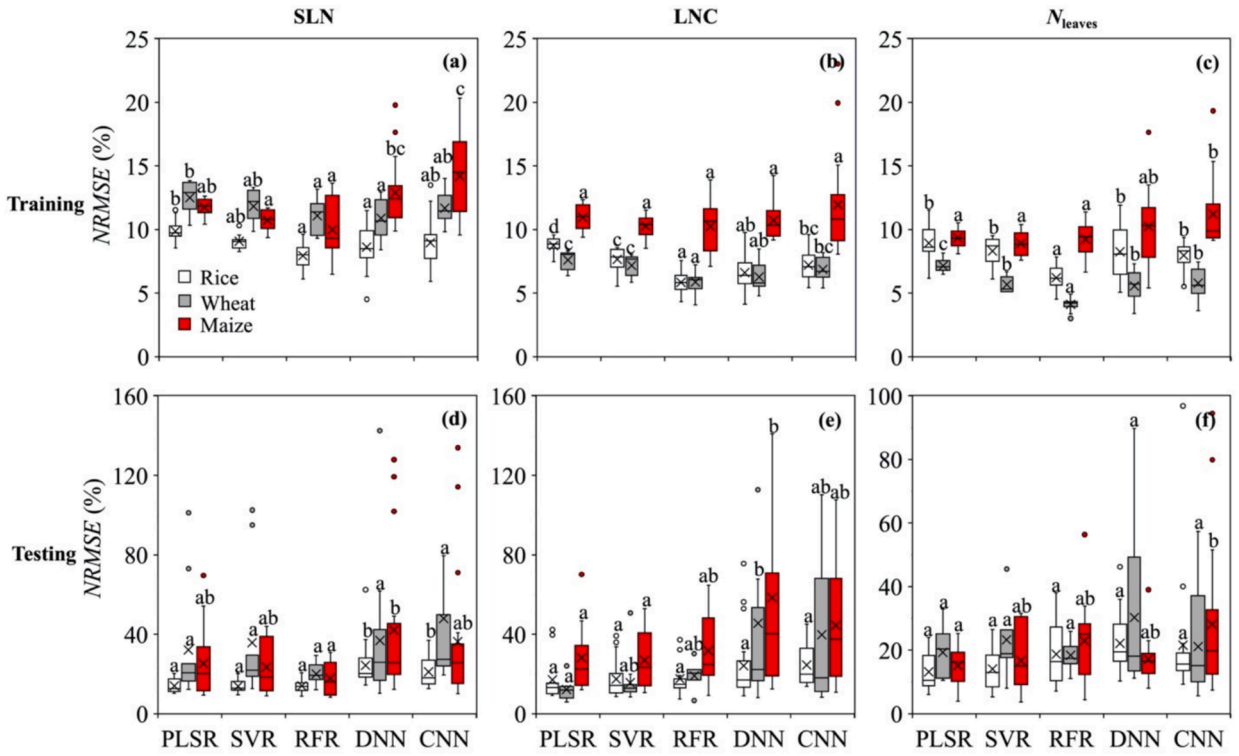

Fig. 6. The prediction performance of different regression models under the procedure of model validation via leave one stage out tests. The boxplots of *NRMSE* of the directly predicted specific leaf nitrogen (SLN) (a, d), leaf nitrogen concentration (LNC) (b, e) and nitrogen content in leaves of the canopy (N_{leaves}) (c, f) are shown in training and testing datasets. All data except for one stage of each crop was used for model training, while the data of the one stage left out was adopted for testing. In each boxplot point, the cross mark represents the mean value, while the vertical spead reprresents the variability, of *NRMSE* arising from all combinations of three feature sets and six leave-out stages. The different letters (a, b and c) above the bars indicate significant differences of prediction performance between regression models according to the HSD Tukey's test. Nonparametric regression algorithms: PLSR = Partial Least Squares Regression, SVR = Support Vector Regression, RFR = Random Forest Regression, DNN = Deep Neural Network, CNN = Convolutional Neural Network. Acronyms in the x-axis for four sets of feature types are defined in Table 3.

3.5. Mapping predicted N_{leaves}

The predicted N_{leaves} values in rice, wheat and maize were mapped in the whole experimental area and illustrated for different growth stages (Fig. 9, Fig. S12-S13). Taking rice as an example, in line with the field measurements (Fig. 3f), the highest N_{leaves} occurred at stem elongation and remarkable differences were shown between experimental plots (Fig. 9b). Such differences among treatments gradually narrowed after stem elongation (Fig. 9b–f). A similar trend was observed in mapped N_{leaves} of wheat (Fig. S12), in agreement with its field measurements (Fig. 3f). In maize, the differences in N_{leaves} among growth stages were predicted well (Fig. S13). The hardly observed differences of predicted N_{leaves} between experimental plots also agreed with the fact that there was no significant difference in measured N_{leaves} between treatments (Fig. 3f, Fig. S13). Moreover, the differences in crop growth status within an experimental plot were also noticeable (Fig. 9, Figs. S12-S13).

4. Discussion

Leaf and canopy N contents across growth stages for three major field crops were predicted from combining different predicting pathways (direct vs. indirect), different hyperspectral image features, and different nonparametric regression algorithms.

4.1. Comparison of direct and indirect predictions

Both SLN and LNC are common leaf level indicators to monitor leaf N. As the components in whole leaf thickness account for the light reflection or absorption, SLN is supposed to be better predicted than LNC (Baret and Fourty, 1997). However, our results showed that the predicted LNC agreed better than the predicted SLN with measurements (Fig. 4a-f, Fig. S8), in line with the previous results of Ecarnot et al. (2013) and Li et al. (2018) using measured raw Ref. Under N shortage, leaf weight increases because of accumulation of starch and cell wall material (McDonald et al., 1986; Terry et al., 1983) and thus SLA or SLW varies significantly (Jones and Hesketh, 1980). As leaf expansion is limited, the change of leaf N status is reflected less in SLN than in LNC. Moreover, as SLN is co-determined from LNC and SLA (or SLW), meaning that it requires more steps to measure SLN than LNC, data for SLN must contain more measurement noise than data for LNC. Despite the better prediction of LNC and SLA, the indirectly predicted SLN_{sla} or SLN_{slw} did not always match measurements better than directly predicted SLN_{dir} (Table 4). Similarly, when upscaling to canopy level, the predicted N_{leaves} from different prediction pathways were comparable (Fig. S11). This result is in contrast with the assertion by Kattenborn et al. (2019) that area-based leaf traits, like SLN, are more suitable for upscaling from leaf to canopy level than mass-based leaf traits, like LNC, as less regression error was introduced. Nevertheless, the selection of upscaling pathways may benefit from exploring the physiological principles. To better clarify the benefits of different prediction pathways, the use of hyperspectral features and the regression processes should be further investigated.

4.2. Contribution of feature types in canopy and leaf nitrogen prediction

Fusing different types of features contributes to plant N traits prediction. Besides the raw bands, VIs have also been considered as supplementary information serving as canopy spectral features (e.g.,

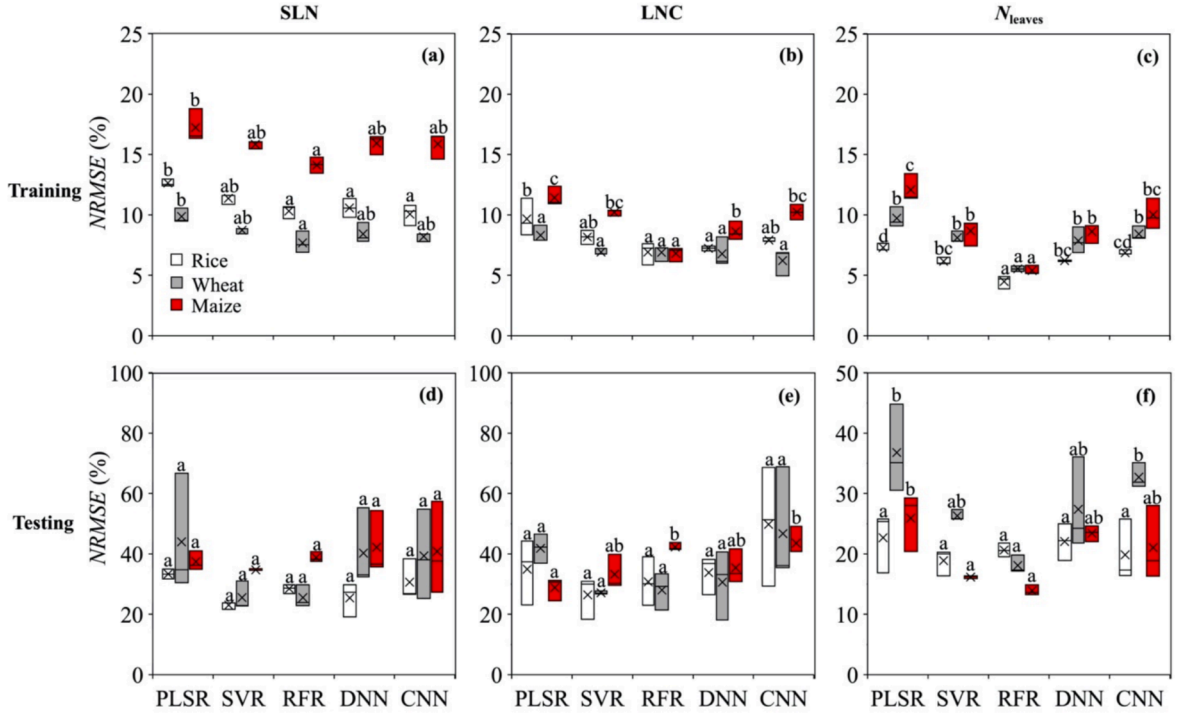

Fig. 7. The prediction performance of different regression models under the procedure of model validation via leave one crop out tests. The boxplots of *NRMSE* of the directly predicted specific leaf nitrogen (SLN) (a, d), leaf nitrogen concentration (LNC) (b, e) and nitrogen content in leaves of the canopy (N_{leaves}) (c, f) are shown in training and testing datasets. The combined data of two crops were used for model training, while the data of the third crop were left for testing. In each boxplot point, the cross mark represents the mean value, while the vertical spread represents the variability, of *NRMSE* arising from all combinations of three feature sets and three leave-out crop species. The different letters (a, b and c) above the bars indicate significant differences of prediction performance between regression models according to the HSD Tukey's test. Nonparametric regression algorithms: PLSR = Partial Least Squares Regression, SVR = Support Vector Regression, RFR = Random Forest Regression, DNN = Deep Neural Network, CNN = Convolutional Neural Network.

Table 4
The prediction performance (*NRMSE*) in the testing dataset of directly and indirectly predicted specific leaf nitrogen (SLN) in rice, wheat and maize using feature sets of Ref, RefTex and RefTexDS (see Table 3 for their definitions) and applying the regression algorithms of Partial Least Squares Regression (PLSR) and Support Vector Regression (SVR) [a].

Crop species	Feature set	PLSR			SVR		
		SLN_{dir}	SLN_{sla}	SLN_{slw}	SLN_{dir}	SLN_{sla}	SLN_{slw}
Rice	Ref	11.3	11.8	12.5	13.4	12.2	12.2
	RefTex	10.7	10.5	10.8	11.1	11.6	11.3
	RefTexDS	10.4	**9.7**	10.3	11.1	9.1	**8.4**
Wheat	Ref	14.4	13.1	13.0	13.2	13.3	13.2
	RefTex	14.2	13.2	12.7	12.8	13.4	12.9
	RefTexDS	14.2	12.5	**12.2**	12.8	12.0	**8.9**
Maize	Ref	14.4	16.9	15.5	16.4	16.9	15.6
	RefTex	16.1	16.1	15.2	17.4	15.9	14.9
	RefTexDS	16.1	11.3	**11.2**	17.4	**10.8**	11.1

[a] For each set of analysis, there is a directly predicted SLN (SLN_{dir}) and two indirectly predicted SLN (SLN_{sla} and SLN_{slw}, see Table 1 for their definitions). In this analysis, the regression algorithm for predicting SLA and SLW required for their respective indirect pathway was always SVR, as it yielded the best performance for the three crops. For the better predicted SLN in the direct vs indirect predictions' comparison, its corresponding *NRMSE* values are given in bold.

Maimaitijiang et al., 2020). There were tight correlations between VIs and leaf N traits (Fig. S4). However, with Ref features used as the baseline, adding VIs to the model did not always yield better prediction in this study (Fig. S6), which might be caused by the introduced noisy information from VIs and/or the correlations between Ref and VIs features. On the other hand, as VIs are normally derived from several bands (Table S2), the information provided from VIs might be limited compared with that from the full-spectrum Ref (Wang et al., 2021). From the extracted canopy texture features, the additional information associated with spatial canopy architecture and structure characteristics is potentially provided (Colombo, 2003). The fusion of canopy Tex benefits the predictions not only of the canopy traits like LAI and biomass (Liu et al., 2021; Zheng et al., 2018b), but also of crop N status like leaf chlorophyll and plant aboveground N content (Qiao et al., 2020; Zheng et al., 2018a). Similar to these previous studies, our results also showed that fusing canopy Tex contributed to the prediction of leaf N traits, especially for the regression models based on PLSR and SVR (Table 4, Fig. 4, Fig. S7). There were also significant ($p < 0.05$) correlations observed between crop structure traits (i.e., LAI and leaf weight) and crop N traits (i.e., LNC, SLN and N_{leaves}) for the three crops (Fig. S14).

Our study successfully estimated crop N and other traits only from visible and NIR regions (Figs. 4 and 7), in line with the results of Baret et al. (2007) and Homolová et al. (2013). Berger et al. (2020b) and Féret et al. (2021) showed that a rational utilization with SWIR region is expected to enhance the prediction of crop N and its seasonal changes. Relying on this, leaf and canopy N traits have been estimated in a promising way via the proxy of proteins, by means of the simulations of the radiative transfer model, PROSAIL-PRO, which distinguishes N-based components (i.e., protein) from carbon-based ones from leaf dry matter content (e.g., Tagliabue et al., 2022; Verrelst et al., 2021). However, it should be noted that the contribution of proteins to either leaf or canopy Ref in the SWIR region is less than 5 %, much smaller than of other input parameters of PROSAIL-PRO, such as carbon-based components and equivalent water thickness (Féret et al., 2021; Wang et al., 2018). The causality of N traits monitoring via leaf and canopy Ref is worthy to be further investigated.

Besides features from hyperspectral sensors, crop DS was

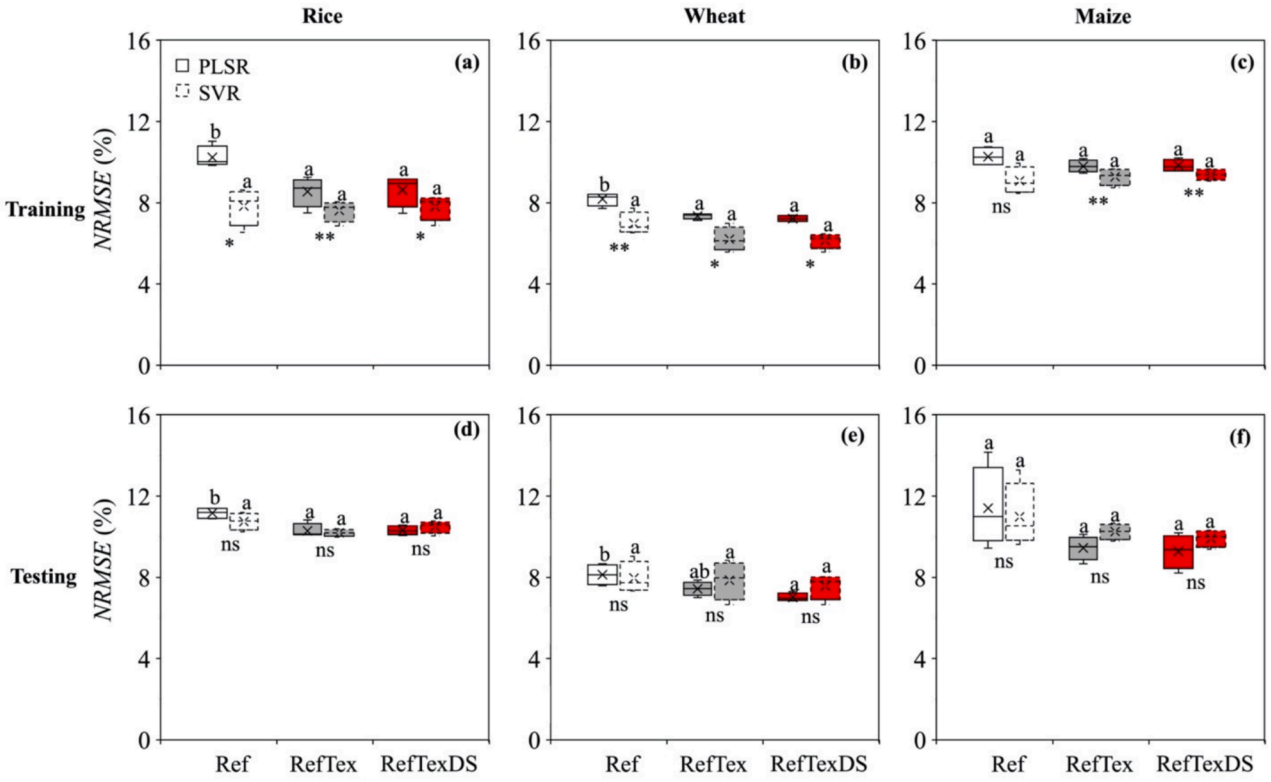

Fig. 8. The prediction performance of different feature sets using regression algorithms of Partial Least Squares Regression (PLSR) and Support Vector Regression (SVR) regarding predicting pathways. The boxplots of *NRMSE* of predicted nitrogen content in leaves of the canopy (N_{leaves}) are shown for rice (a, d), wheat (b, e) and maize (c, f) in the training and testing datasets. In each boxplot point, the cross mark represents the mean value, while the vertical spread represents the variability, of *NRMSE* arising from using the four prediction pathways. The different letters (a, b and c) above the bars indicate significant differences of prediction performance between regression models according to the HSD Tukey's test. The significance of the difference between the prediction performance using regression algorithms of PLSR and SVR is presented as ns (not significant), * ($p < 0.05$) and ** ($p < 0.01$), respectively, according to the Student's *t*-test. Acronyms in the x-axis for three sets of feature types are defined in Table 3.

additionally examined to enhance the prediction. Crop N demand changes during the vegetative and reproductive phases, while N movement and reallocating within the crop occur as well (Ohyama, 2010). The observed LNC decreased with crop growth (Fig. 3e). Affected by biomass accumulation, SLN tended to decrease monotonically as well, while the change of N_{leaves} followed a bell-shaped curve (Fig. 3d, f). Thus, as both measured canopy Ref and leaf N traits changed across growth stages (Fig. 3), the performance of the regressing models in predicting leaf N traits improved after incorporating DS into the models, although the improvements were not always significant (Table 4, Figs. 4 and 8). Nevertheless, Li et al. (2022) found that the slopes and intercepts of ordinary least squares regression of aboveground biomass in wheat with VIs had a strong relationship with DS. This suggests that the appropriate digital indicator of crop growth stages is of importance. The simulated DS in our study is only one way of quantifying DS, using a bell-shaped temperature response function (see Supplement Text A). It is similar to growth stages in the Zadoks scale, using numeric codes between 0 and 100 representing stages from sowing to harvest (Zadoks et al., 1974). As growth stages from the Zadoks scale are difficult to acquire over large areas, the DS regarding crop temperature response in this study is recommended for follow-up research.

4.3. Characteristics of regression algorithms in canopy and leaf nitrogen prediction

The performance of five popular nonparametric regression algorithms was evaluated for N traits in three major field crops in this study. Among these methods, PLSR used the least number of hyperparameters and SVR next to it, compared with RFR, DNN and CNN that had many hyperparameters (Table S4) and thus, in principle, should have more flexibility in the prediction of leaf N traits. However, our results showed that PLSR and SVR tended to be more stable and PLSR was likely to achieve the best performance in the prediction of N_{leaves}, as well as SLN and LNC (Figs. 4 and 8), in line with the results in the prediction of LNC in wheat (Yao et al., 2015). This might be caused by the limited size of our dataset, as PLSR is known to be more effective than others, when the number of samples is smaller than the number of variables (Geladi and Kowalski, 1986). With nearly 1000 samples, DNN-based yield prediction models systematically performed better than PLSR- and SVR-based models while increasing feature types (Maimaitijiang et al., 2020). Moreover, with more than 7000 samples from different years and locations, CNN provided higher accuracy than PLSR in LNC prediction in grass (Pullanagari et al., 2021). Thus, as the numerous combinations of hyperparameters in RFR and of hidden layers and neuro numbers in DNN and CNN have already been trialed in this study (Table S4, Fig. S1), increasing the number of samples might be the essential for improving the predictability of DNN and CNN.

4.4. Other considerations for the prediction of crop nitrogen traits

We tested the transferability of the trained models using hyperspectral features and DS for predicting N_{leaves} across crop species or across stages. Dai et al. (2023) showed the good performance of the PSLR model in predicting LNC across sites and crop species, yet its transferability to crop species outside the training set was not verified. In line with this, our results also concluded that the PLSR model performed better in predicting both canopy and leaf N traits across crop species and growth stages (Figs. 5 and 6). However, this finding should be cautiously

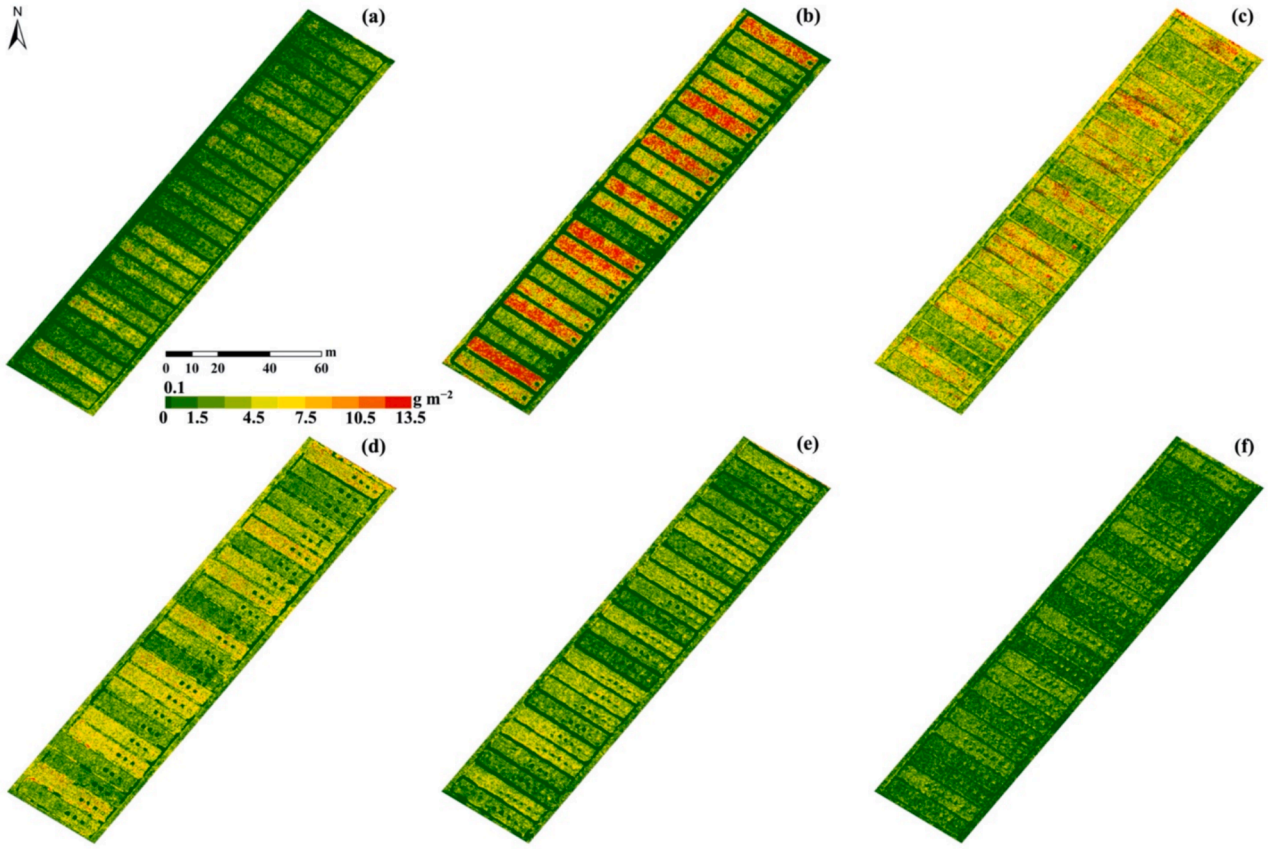

Fig. 9. The predicted nitrogen content in leaves of the canopy (N_{leaves}) from its direct predictions $N_{leaves,dir}$ (see Table 1 for its definition) at the experimental area of rice across the whole growing season using feature set of RefTexDS (see Table 3 for its definition) and regression algorithm of Partial Least Squares Regression. Predicted $N_{leaves,dir}$ at the stage of tillering (a), stem-elongating (b), flowering (c), about 15 days after flowering (d), about 30 days after flowering (e), and maturity (f) are shown.

generalized, because the collected dataset was limited to one year and one site per crop in our study. To cope with the temporal and spatial differences across covered regions, a data fusing method for satellite images with different resolutions has been developed to achieve high spatial resolution (Zhu et al., 2016). This may also empower the potential to effectively exploit texture information in satellite images with coarse resolution and mixed pixels. Alternatively, instead of collecting field data across sites, regions and years, the deep learning model can be pre-trained with simulated data from process-based models and fine-tuned with a few in-situ field samples (Ma et al., 2024). For instance, a radiative transfer model-based method has also been developed for predicting SLN and N_{leaves} for different crop and grass species in different sites (Boegh et al., 2013). For more accurate predictions of crop N traits, hybrid methods that combine radiative transfer models and nonparametric regression algorithms are suggested (Dai et al., 2023).

Relying on the continuous spectral coverage, the hyperspectral sensors are more likely to capture the subtle spectral signatures than the multispectral ones and are therefore preferred for monitoring crop N (Berger et al., 2020a). However, model predictability can also be affected by the autocorrelation of features within obtained hyperspectral data. Our results showed that the PLSR model can better manage this autocorrelation (see an earlier section), and thus gave a better performance than other models (Figs. 5 and 8). Thus, the reduction of feature space while preserving the original information may be necessary (Rivera-Caicedo et al., 2017; Liu et al., 2024a; Liu et al., 2024b). Normally, most information can be covered within the first several components, but a high number of components may still be required for subtle but relevant information, along with the included noisy information (Candiani et al., 2022; Verrelst et al., 2021). Moreover, the original meaning of the features may no longer be kept after transformation (Wu et al., 2007). On the other hand, the method of feature selection enables model construction via a subset of relevant features without changing their original meaning. Yet, the identified features might differ, because of confounding factors between the leaf and canopy Ref (Berger et al., 2020a; Féret et al., 2021). Hence, relevant studies are needed to optimize the tradeoff among feature selection and transformation, feature meaning relevance, and model predictability.

5. Conclusions

On the basis of synthesizing available information, we evaluated the prediction of area- and mass-based leaf N traits using combined hyperspectral features and DS, different regression algorithms and different prediction pathways for three major crops, rice, wheat and maize. We showed that for the prediction of N traits at leaf level (SLN and LNC) and at canopy level (N_{leaves}) using a data set of limited size, regression algorithms of PLSR and SVR tended to perform better than others, and the incorporation of different types of features, like canopy Ref, Tex and DS, helped improve model performance. The regression algorithm of PLSR performed slightly better than SVR in the prediction of N_{leaves}. Like the predicted SLN, the predictions of N_{leaves} from direct and indirect pathways performed comparably. These results provide useful information for a next-step work, e.g., that couples the real-time accurately retrieved leaf and canopy N traits into dynamic crop models so as to predict the real-time growth status more accurately. This would better enable to guide farmers for in situ field N management targeting the maximal yield or resource use efficiency.

CRediT authorship contribution statement

Dong Wang: Writing – review & editing, Writing – original draft, Formal analysis, Data curation, Conceptualization. **Paul C. Struik:** Writing – review & editing, Supervision, Formal analysis, Conceptualization. **Lei Liang:** Supervision, Software, Formal analysis. **Xinyou Yin:** Writing – review & editing, Supervision, Formal analysis, Conceptualization.

Declaration of competing interest

The authors declare the following financial interests/personal relationships which may be considered as potential competing interests: [Dong Wang reports a relationship with Shanghai Lankuaikei Technology Development Co. Ltd. that includes: employment. Lei Liang reports a relationship with Shanghai Lankuaikei Technology Development Co. Ltd. that includes: employment].

Acknowledgment

We acknowledge the financial support from the High-tech Industry and Scientific and Technological Innovation Project of Lin-gang Special Area, Shanghai (grant number: SH-LG-GK-2020-02-19).

Appendix A. Supplementary data

Supplementary data to this article can be found online at https://doi.org/10.1016/j.compag.2025.110147.

Data availability

The authors do not have permission to share data.

References

Abadi, M., Agarwal, A., Barham, P., Brevdo, E., Chen, Z., Citro. Craig, Corrado, G. S., Davis, A., Dean, J., Devin, M., Ghemawat, S., Goodfellow, I., Harp, A., Irving, G., Isard, M., Jozefowicz, R., Jia, Y., Kaiser, L., Kudlur, M., Levenberg, J., Mané, D., Schuster, M., Monga, R., Moore, S., Murray, D., Olah, C., Shlens, J., Steiner, B., Sutskever, I., Talwar, K., Tucker, P., Vanhoucke, V., Vasudevan, V., Viégas, F., Vinyals, O., Warden, P., Wattenberg, M., Wicke, M., Yu, Y., Zheng, X. (2015). TensorFlow: A System for Large-Scale Machine Learning. Software available from tensflow.org.

Aasen, H., Burkart, A., Bolten, A., Bareth, G., 2015. Generating 3D hyperspectral information with lightweight UAV snapshot cameras for vegetation monitoring: from camera calibration to quality assurance. ISPRS Journal of Photogrammetry and Remote Sensing 108, 245–259. https://doi.org/10.1016/j.isprsjprs.2015.08.002.

Atzberger, C., Guérif, M., Baret, F., Werner, W., 2010. Comparative analysis of three chemometric techniques for the spectroradiometric assessment of canopy chlorophyll content in winter wheat. Comput. Electron. Agric. 73, 165–173. https://doi.org/10.1016/j.compag.2010.05.006.

Barbedo, J.G.A., 2019. Detection of nutrition deficiencies in plants using proximal images and machine learning: a review. Comput. Electron. Agric. 162, 482–492. https://doi.org/10.1016/j.compag.2019.04.035.

Baret, F., Fourty, T., 1997. Radiometric estimates of nitrogen status of leaves and canopies. In: Lemaire, G. (Ed.), Diagnosis of nitrogen status in crops. Springer, pp. 201–227.

Baret, F., Houles, V., Guerif, M., 2007. Quantification of plant stress using remote sensing observations and crop models: the case of nitrogen management. J. Exp. Bot. 58, 869–880. https://doi.org/10.1093/jxb/erl231.

Beeckman, F., Motte, H., Beeckman, T., 2018. Nitrification in agricultural soils: impact, actors and mitigation. Curr. Opin. Biotechnol. 50, 166–173.

Berger, K., Verrelst, J., Féret, J.-B., Hank, T., Wocher, M., Mauser, W., Camps-Valls, G., 2020a. Retrieval of aboveground crop nitrogen content with a hybrid machine learning method. Int. J. Appl. Earth Obs. Geoinf. 92, 102174. https://doi.org/10.1016/j.jag.2020.102174.

Berger, K., Verrelst, J., Féret, J.-B., Wang, Z., Wocher, M., Strathmann, M., Danner, M., Mauser, W., Hank, T., 2020b. Crop nitrogen monitoring: recent progress and principal developments in the context of imaging spectroscopy missions. Remote Sens. Environ. 242, 111758. https://doi.org/10.1016/j.rse.2020.111758.

Blackburn, G.A., 1998. Quantifying chlorophylls and caroteniods at leaf and canopy scales: an evaluation of some hyperspectral approaches. Remote Sens. Environ. 66, 273–285.

Boegh, E., Houborg, R., Bienkowski, J., Braban, C.F., Dalgaard, T., van Dijk, N., Dragosits, U., Holmes, E., Magliulo, V., Schelde, K., Di Tommasi, P., Vitale, L., Theobald, M.R., Cellier, P., Sutton, M.A., 2013. Remote sensing of LAI, chlorophyll and leaf nitrogen pools of crop- and grasslands in five European landscapes. Biogeosciences 10, 6279–6307. https://doi.org/10.5194/bg-10-6279-2013.

Breiman, L., 2001. Random forests. Mach. Learn. 45, 5–32.

Candiani, G., Tagliabue, G., Panigada, C., Verrelst, J., Picchi, V., Caicedo, J.P.R., Boschetti, M., 2022. Evaluation of hybrid models to estimate chlorophyll and nitrogen content of maize crops in the framework of the future CHIME mission. Remote Sens. (Basel) 14, 1792. https://doi.org/10.3390/rs14081792.

Chen, X.P., Cui, Z.L., Vitousek, P.M., Cassman, K.G., Matson, P.A., Bai, J.S., Meng, Q.F., Hou, P., Yue, S.C., Romheld, V., Zhang, F.S., 2011. Integrated soil-crop system management for food security. PNAS 108, 6399–6404. https://doi.org/10.1073/pnas.1101419108.

Colombo, R., 2003. Retrieval of leaf area index in different vegetation types using high resolution satellite data. Remote Sens. Environ. 86, 120–131. https://doi.org/10.1016/s0034-4257(03)00094-4.

Dai, J., Jamalinia, E., Vaughn, N.R., Martin, R.E., König, M., Hondula, K.L., Calhoun, J., Heckler, J., Asner, G.P., 2023. A general methodology for the quantification of crop canopy nitrogen across diverse species using airborne imaging spectroscopy. Remote Sens. Environ. 298. https://doi.org/10.1016/j.rse.2023.113836.

Davidson, E.A., 2009. The contribution of manure and fertilizer nitrogen to atmospheric nitrous oxide since 1860. Nat. Geosci. 2, 659–662.

Drucker, H., Burges, C.J., Kaufman, L., Smola, A., Vapnik, V., 1997. Support vector regression machines. In: Mozer, M., Jordan, J., Petscbe, T. (Eds.), Neural Information Processing Systems 9. MIT Press, Cambridge, MA, pp. 155–161.

Ecarnot, M., Compan, F., Roumet, P., 2013. Assessing leaf nitrogen content and leaf mass per unit area of wheat in the field throughout plant cycle with a portable spectrometer. Field Crop Res 140, 44–50. https://doi.org/10.1016/j.fcr.2012.10.013.

Evans, J.R., 1983. Nitrogen and photosynthesis in the flag leaf of wheat (Triticum aestivum L.). Plant Physiol. 72, 297–302.

FAO. (2020). *World Food and Agriculture - Statistical Yearbook 2020*. Rome.

Féret, J.-B., Berger, K., de Boissieu, F., Malenovský, Z., 2021. PROSPECT-PRO for estimating content of nitrogen-containing leaf proteins and other carbon-based constituents. Remote Sens. Environ. 252, 112173. https://doi.org/10.1016/j.rse.2020.112173.

Fu, Y., Yang, G., Li, Z., Li, H., Li, Z., Xu, X., Song, X., Zhang, Y., Duan, D., Zhao, C., Chen, L., 2020. Progress of hyperspectral data processing and modelling for cereal crop nitrogen monitoring. Comput. Electron. Agric. 172, 105321. https://doi.org/10.1016/j.compag.2020.105321.

Geladi, P., Kowalski, B.R., 1986. Partial least-squares regression: a tutorial. Anal. Chim. Acta 185, 1–17.

Guanter, L., Kaufmann, H., Segl, K., Foerster, S., Rogass, C., Chabrillat, S., Kuester, T., Hollstein, A., Rossner, G., Chlebek, C., Straif, C., Fischer, S., Schrader, S., Storch, T., Heiden, U., Mueller, A., Bachmann, M., Mühle, H., Müller, R., Habermeyer, M., Ohndorf, A., Hill, J., Buddenbaum, H., Hostert, P., van der Linden, S., Leitão, P., Rabe, A., Doerffer, R., Krasemann, H., Xi, H., Mauser, W., Hank, T., Locherer, M., Rast, M., Staenz, K., Sang, B., 2015. The EnMAP spaceborne imaging spectroscopy mission for earth observation. Remote Sens. (Basel) 7, 8830–8857. https://doi.org/10.3390/rs70708830.

Haralick, R.M., Shanmugam, K., Dinstein, I.H., 1973. Textural features for image classification. IEEE Trans. Syst. Man Cybern. 610–621.

He, K., Zhang, X., Ren, S., Sun, J. (2015). *Delving deep into rectifiers: Surpassing human-level performance on imagenet classification.*

Homolová, L., Malenovský, Z., Clevers, J.G.P.W., García-Santos, G., Schaepman, M.E., 2013. Review of optical-based remote sensing for plant trait mapping. Ecol. Complex. 15, 1–16. https://doi.org/10.1016/j.ecocom.2013.06.003.

Horler, D.N.H., Dockray, M., Barber, J., 1983. The red edge of plant leaf reflectance. Int. J. Remote Sens. 4, 273–288.

Jones, J.W., Hesketh, J.D., 1980. Predicting leaf expansion. In: Hesketh, J.D., Jones, J.W. (Eds.), Predicting Photosynthesis for Ecosystem Models, Volume II. CRC Press, Boca Raton, FL, pp. 85–122.

Kattenborn, T., Schiefer, F., Zarco-Tejada, P., Schmidtlein, S., 2019. Advantages of retrieving pigment content [μg/cm^2] versus concentration [%] from canopy reflectance. Remote Sens. Environ. 230. https://doi.org/10.1016/j.rse.2019.05.014.

Kokaly, R.F., Asner, G.P., Ollinger, S.V., Martin, M.E., Wessman, C.A., 2009. Characterizing canopy biochemistry from imaging spectroscopy and its application to ecosystem studies. Remote Sens. Environ. 113, S78–S91. https://doi.org/10.1016/j.rse.2008.10.018.

Längkvist, M., Karlsson, L., Loutfi, A., 2014. A review of unsupervised feature learning and deep learning for time-series modeling. Pattern Recogn. Lett. 42, 11–24. https://doi.org/10.1016/j.patrec.2014.01.008.

LeCun, Y., Bengio, Y., Hinton, G., 2015. Deep learning. Nature 521, 436–444. https://doi.org/10.1038/nature14539.

Lemaire, G., Jeuffroy, M.-H., Gastal, F., 2008. Diagnosis tool for plant and crop N status in vegetative stage: theory and practices for crop N management. Eur. J. Agron. 28, 614–624. https://doi.org/10.1016/j.eja.2008.01.005.

Li, D., Wang, X., Zheng, H., Zhou, K., Yao, X., Tian, Y., Zhu, Y., Cao, W., Cheng, T., 2018. Estimation of area- and mass-based leaf nitrogen contents of wheat and rice crops from water-removed spectra using continuous wavelet analysis. Plant Methods 14, 76. https://doi.org/10.1186/s13007-018-0344-1.

Li, Z., Zhao, Y., Taylor, J., Gaulton, R., Jin, X., Song, X., Li, Z., Meng, Y., Chen, P., Feng, H., Wang, C., Guo, W., Xu, X., Chen, L., Yang, G., 2022. Comparison and transferability of thermal, temporal and phenological-based in-season predictions of above-ground biomass in wheat crops from proximal crop reflectance data. Remote Sens. Environ. 273, 112967. https://doi.org/10.1016/j.rse.2022.112967.

Liu, S., Jin, X., Nie, C., Wang, S., Yu, X., Cheng, M., Shao, M., Wang, Z., Tuohuti, N., Bai, Y., Liu, Y., 2021. Estimating leaf area index using unmanned aerial vehicle data: shallow vs. deep machine learning algorithms. Plant Physiol. 187, 1551–1576. https://doi.org/10.1093/plphys/kiab322.

Liu, Y., Feng, H., Fan, Y., Yue, J., Chen, R., Ma, Y., Bian, M., Yang, G., 2024a. Improving potato above ground biomass estimation combining hyperspectral data and harmonic decomposition techniques. Comput. Electron. Agric. 218. https://doi.org/10.1016/j.compag.2024.108699.

Liu, Y., Feng, H., Yue, J., Jin, X., Fan, Y., Chen, R., Bian, M., Ma, Y., Li, J., Xu, B., Yang, G., 2024b. Improving potato AGB estimation to mitigate phenological stage impacts through depth features from hyperspectral data. Comput. Electron. Agric. 219. https://doi.org/10.1016/j.compag.2024.108808.

Liu, Y., Feng, H., Yue, J., Li, Z., Yang, G., Song, X., Yang, X., Zhao, Y., 2022. Remote-sensing estimation of potato above-ground biomass based on spectral and spatial features extracted from high-definition digital camera images. Comput. Electron. Agric. 198, 107089. https://doi.org/10.1016/j.compag.2022.107089.

Lu, J., Li, W., Yu, M., Zhang, X., Ma, Y., Su, X., Yao, X., Cheng, T., Zhu, Y., Cao, W., Tian, Y., 2020. Estimation of rice plant potassium accumulation based on non-negative matrix factorization using hyperspectral reflectance. Precis. Agric. 22, 51–74. https://doi.org/10.1007/s11119-020-09729-z.

Ma, Y., Chen, S., Ermon, S., Lobell, D.B., 2024. Transfer learning in environmental remote sensing. Remote Sens. Environ. 301, 113924. https://doi.org/10.1016/j.rse.2023.113924.

Maimaitijiang, M., Sagan, V., Sidike, P., Hartling, S., Esposito, F., Fritschi, F.B., 2020. Soybean yield prediction from UAV using multimodal data fusion and deep learning. Remote Sens. Environ. 237, 111599. https://doi.org/10.1016/j.rse.2019.111599.

McDonald, A.J.S., Lohammar, T., Ericsson, A., 1986. Growth response to step-decrease in nutrient availability in small birch (Betula pendula Roth). Plant Cell Environ. 9, 427–432.

Miller, J.R., Hare, E.W., Wu, J., 1990. Quantitative characterization of the vegetation red edge reflectance 1. An inverted-Gaussian reflectance model. Int. J. Remote Sens. 11, 1755–1773. https://doi.org/10.1080/01431169008955128.

Moharana, S., Dutta, S., 2016. Spatial variability of chlorophyll and nitrogen content of rice from hyperspectral imagery. ISPRS J. Photogramm. Remote Sens. 122, 17–29. https://doi.org/10.1016/j.isprsjprs.2016.09.002.

Ohyama, T., 2010. Nitrogen as a major essential element of plants. In: Ohyama, T., Sueyoshi, K. (Eds.), *Nitrogen Assimilation in Plants*. Research Signpost, pp. 1–18.

Padilla, F.M., Gallardo, M., Manzano-Agugliaro, F., 2018. Global trends in nitrate leaching research in the 1960–2017 period. Sci. Total Environ. 643, 400–413.

Pedregosa, F., Varoquaux, G., Gramfort, A., Michel, V., Thirion, B., Grisel, O., Blondel, M., Prettenhofer, P., Weiss, R., Dubourg, V., Vanderplas, J., Passos, A., Cournapeau, D., Brucher, M., Perrot, M., Duchesnay, E., 2011. Scikit-learn: machine learning in python. J. Mach. Learn. Res. 2825–2830.

Peng, S., Cassman, K.G., Kropff, M.J., 1995. Relationship between leaf photosynthesis and nitrogen content of field-grown rice in tropics. Crop Sci. 35, 1627–1630.

Pullanagari, R.R., Dehghan-Shoar, M., Yule, I.J., Bhatia, N., 2021. Field spectroscopy of canopy nitrogen concentration in temperate grasslands using a convolutional neural network. Remote Sens. Environ. 257, 112353. https://doi.org/10.1016/j.rse.2021.112353.

Qiao, L., Gao, D., Zhang, J., Li, M., Sun, H., Ma, J., 2020. Dynamic influence elimination and chlorophyll content diagnosis of maize using UAV spectral imagery. Remote Sens. (Basel) 12 (16). https://doi.org/10.3390/rs12162650.

Raj, R., Walker, J.P., Pingale, R., Banoth, B.N., Jagarlapudi, A., 2021. Leaf nitrogen content estimation using top-of-canopy airborne hyperspectral data. Int. J. Appl. Earth Obs. Geoinf. 104, 102584. https://doi.org/10.1016/j.jag.2021.102584.

Rivera-Caicedo, J.P., Verrelst, J., Muñoz-Marí, J., Camps-Valls, G., Moreno, J., 2017. Hyperspectral dimensionality reduction for biophysical variable statistical retrieval. ISPRS J. Photogramm. Remote Sens. 132, 88–101. https://doi.org/10.1016/j.isprsjprs.2017.08.012.

Schröder, J.J., Neeteson, J.J., Oenema, O., Struik, P.C., 2000. Does the crop or the soil indicate how to save nitrogen in maize production?: Reviewing the state of the art. Field Crop Res 66, 151–164.

Skiba, U.M., 2014. Nitrous oxide, climate change and agriculture. CAB Reviews: Perspectives in Agriculture, Veterinary Science, Nutrition and Natural Resources 9. https://doi.org/10.1079/pavsnnr20149010.

Tagliabue, G., Boschetti, M., Bramati, G., Candiani, G., Colombo, R., Nutini, F., Pompilio, L., Rivera-Caicedo, J.P., Rossi, M., Rossini, M., Verrelst, J., Panigada, C., 2022. Hybrid retrieval of crop traits from multi-temporal PRISMA hyperspectral imagery. ISPRS Journal of Photogrammetry and Remote Sensing 187, 362–377. https://doi.org/10.1016/j.isprsjprs.2022.03.014.

Terry, N., Waldron, L.J., Taylor, S.E., 1983. Environmental influences on leaf expansion. In: Dale, J.E., Milthorpe, F.L. (Eds.), The Growth and Functioning of Leaves. Cambridge University Press, Cambridge, pp. 179–205.

Thomas, J.R., Oerther, G.F., 1972. Estimating nitrogen content of sweet pepper leaves by reflectance measurements. Agron. J. 64, 11–13.

Verrelst, J., Malenovský, Z., Van der Tol, C., Camps-Valls, G., Gastellu-Etchegorry, J.-P., Lewis, P., North, P., Moreno, J., 2019. Quantifying vegetation biophysical variables from imaging spectroscopy data: a review on retrieval methods. Surv. Geophys. 40, 589–629. https://doi.org/10.1007/s10712-018-9478-y.

Verrelst, J., Rivera-Caicedo, J.P., Reyes-Munoz, P., Morata, M., Amin, E., Tagliabue, G., Panigada, C., Hank, T., Berger, K., 2021. Mapping landscape canopy nitrogen content from space using PRISMA data. ISPRS J. Photogramm. Remote Sens. 178, 382–395. https://doi.org/10.1016/j.isprsjprs.2021.06.017.

Wang, D., Rianti, W., Gálvez, F., van der Putten, P.E.L., Struik, P.C., Yin, X., 2022. Estimating photosynthetic parameter values of rice, wheat, maize and sorghum to enable smart crop cultivation. Crop Environ. 1 (2), 119–132. https://doi.org/10.1016/j.crope.2022.05.004.

Wang, L., Chen, S., Li, D., Wang, C., Jiang, H., Zheng, Q., Peng, Z., 2021. Estimation of paddy rice nitrogen content and accumulation both at leaf and plant levels from UAV hyperspectral imagery. Remote Sens. (Basel) 13, 2956. https://doi.org/10.3390/rs13152956.

Wang, Z., Skidmore, A.K., Darvishzadeh, R., Wang, T., 2018. Mapping forest canopy nitrogen content by inversion of coupled leaf-canopy radiative transfer models from airborne hyperspectral imagery. Agric. For. Meteorol. 253–254, 247–260. https://doi.org/10.1016/j.agrformet.2018.02.010.

Wu, X., Kumar, V., Ross Quinlan, J., Ghosh, J., Yang, Q., Motoda, H., McLachlan, G.J., Ng, A., Liu, B., Yu, P.S., Zhou, Z.-H., Steinbach, M., Hand, D.J., Steinberg, D., 2007. Top 10 algorithms in data mining. Knowl. Inf. Syst. 14, 1–37. https://doi.org/10.1007/s10115-007-0114-2.

Weiss, M., Jacob, F., Duveiller, G., 2020. Remote sensing for agricultural applications: a meta-review. Remote Sens. Environ. 236, 111402.

Yao, X., Huang, Y., Shang, G., Zhou, C., Cheng, T., Tian, Y., Cao, W., Zhu, Y., 2015. Evaluation of six algorithms to monitor wheat leaf nitrogen concentration. Remote Sens. (Basel) 7, 14939–14966. https://doi.org/10.3390/rs71114939.

Yin, X., Struik, P.C., 2017. Can increased leaf photosynthesis be converted into higher crop mass production? A simulation study for rice using the crop model GECROS. J. Exp. Bot. 68, 2345–2360. https://doi.org/10.1093/jxb/erx085.

Yin, X., Struik, P.C., Romero, P., Harbinson, J., Evers, J.B., PE, D. P, V., Vos, J., 2009. Using combined measurements of gas exchange and chlorophyll fluorescence to estimate parameters of a biochemical C3 photosynthesis model: a critical appraisal and a new integrated approach applied to leaves in a wheat (Triticum aestivum) canopy. Plant Cell Environ. 32, 448–464. https://doi.org/10.1111/j.1365-3040.2009.01934.x.

Yin, X., van Laar, H.H., 2005. *Crop systems dynamics: an ecophysiological simulation model for genotype-by-environment interactions*. Wageningen Academic Publishers, Wageningen, the Netherlands.

Zadoks, J.C., Chang, T.T., Konzak, C.F., 1974. A decimal code for the growth stages of cereals. Weed Res. 14, 415–421.

Zeng, F., Zuo, Z., Mo, J., Chen, C., Yang, X., Wang, J., Wang, Y., Zhao, Z., Chen, T., Li, Y., Zhang, Z., Hu, Z., Xu, H., 2021. Runoff losses in nitrogen and phosphorus from paddy and maize cropping systems: a field study in Dongjiang Basin, South China. Frontiers in Plant Science 12, 675121. https://doi.org/10.3389/fpls.2021.675121.

Zhang, F., Chen, X., Vitousek, P., 2013. Chinese agriculture: An experiment for the world. Nature 497 (7447), 33–35.

Zheng, H., Cheng, T., Li, D., Yao, X., Tian, Y., Cao, W., Zhu, Y., 2018a. Combining Unmanned Aerial Vehicle (UAV)-based multispectral imagery and ground-based hyperspectral data for plant nitrogen concentration estimation in rice. Front. Plant Sci. 9, 936. https://doi.org/10.3389/fpls.2018.00936.

Zheng, H., Cheng, T., Zhou, M., Li, D., Yao, X., Tian, Y., Cao, W., Zhu, Y., 2018b. Improved estimation of rice aboveground biomass combining textural and spectral analysis of UAV imagery. Precis. Agric. 20, 611–629. https://doi.org/10.1007/s11119-018-9600-7.

Zhu, X., Helmer, E.H., Gao, F., Liu, D., Chen, J., Lefsky, M.A., 2016. A flexible spatiotemporal method for fusing satellite images with different resolutions. Remote Sens. Environ. 172, 165–177. https://doi.org/10.1016/j.rse.2015.11.016.